EUROPEAN ORGANIZATION FOR NUCLEAR RESEARCH

CERN–PPE/95-08

17 January 1995

Measurement of $\frac{\Gamma_{b\bar{b}}}{\Gamma_{had}}$ using Impact Parameter Measurements and Lepton Identification

DELPHI Collaboration

Abstract

The partial decay width of the Z to $b\overline{b}$ quark pairs has been measured by the DELPHI detector at LEP. b-hadrons, containing b-quarks, were tagged by leptons with high transverse momentum relative to the hadron or by tracks with large impact parameters to the primary vertex.
The ratio of the numbers of events with a single such tag to those with two tags was used to estimate the efficiency of the method and to reduce the systematic uncertainty. Combining all methods, the value:

$$\frac{\Gamma_{b\bar{b}}}{\Gamma_{had}} = 0.2210 \pm 0.0033 \pm 0.0003(model) \pm 0.0014(\Gamma_{c\bar{c}})$$

was found, where the third error corresponds to a $\pm 8\%$ uncertainty on the $c\overline{c}$ production width. A maximum likelihood fit to the single and di-lepton distributions gave the branching fraction of the decays of b-quarks to leptons as:

$$BR(b \to l) = (11.06 \pm 0.39 \pm 0.19(model) \pm 0.12(\Gamma_{c\bar{c}}))\,\%.$$

(To be submitted to Zeit. f. Physik C)

P.Abreu[21], W.Adam[8], T.Adye[38], E.Agasi[31], I.Ajinenko[43], R.Aleksan[40], G.D.Alekseev[15], P.P.Allport[22], S.Almehed[24], F.M.L.Almeida[48], S.J.Alvsvaag[4], U.Amaldi[8], S.Amato[48], A.Andreazza[28], M.L.Andrieux[13], P.Antilogus[25], W-D.Apel[16], Y.Arnoud[40], B.Åsman[45], J-E.Augustin[19], A.Augustinus[31], P.Baillon[8], P.Bambade[19], F.Barao[21], R.Barate[13], D.Y.Bardin[15], G.J.Barker[35], A.Baroncelli[41], O.Barring[8], J.A.Barrio[26], W.Bartl[51], M.J.Bates[38], M.Battaglia[14], M.Baubillier[23], J.Baudot[40], K-H.Becks[53], M.Begalli[37], P.Beilliere[7], Yu.Belokopytov[8], P.Beltran[10], A.C.Benvenuti[5], M.Berggren[42], D.Bertrand[2], F.Bianchi[46], M.Bigi[46], M.S.Bilenky[15], P.Billoir[23], J.Bjarne[24], D.Bloch[9], M.Blume[53], S.Blyth[35], V.Bocci[39], T.Bolognese[40], M.Bonesini[28], W.Bonivento[28], P.S.L.Booth[22], G.Borisov[43], C.Bosio[41], B.Bostjancic[44], S.Bosworth[35], O.Botner[49], E.Boudinov[43], B.Bouquet[19], C.Bourdarios[19], T.J.V.Bowcock[22], M.Bozzo[12], P.Branchini[41], K.D.Brand[36], R.A.Brenner[14], H.Briand[23], C.Bricman[2], L.Brillault[23], R.C.A.Brown[8], P.Bruckman[17], J-M.Brunet[7], L.Bugge[33], T.Buran[33], A.Buys[8], M.Caccia[28], M.Calvi[28], A.J.Camacho Rozas[42], T.Camporesi[8], V.Canale[39], M.Canepa[12], K.Cankocak[45], F.Cao[2], F.Carena[8], P.Carrilho[48], L.Carroll[22], C.Caso[12], V.Cassio[46], M.V.Castillo Gimenez[50], A.Cattai[8], F.R.Cavallo[5], L.Cerrito[39], V.Chabaud[8], A.Chan[1], Ph.Charpentier[8], L.Chaussard[25], J.Chauveau[23], P.Checchia[36], G.A.Chelkov[15], P.Chliapnikov[43], P.Chochula[6], V.Chorowicz[8], J.T.M.Chrin[50], V.Cindro[44], P.Collins[35], J.L.Contreras[19], R.Contri[12], E.Cortina[50], G.Cosme[19], F.Cossutti[47], H.B.Crawley[1], D.Crennell[38], G.Crosetti[12], J.Cuevas Maestro[34], S.Czellar[14], E.Dahl-Jensen[29], J.Dahm[53], B.Dalmagne[19], M.Dam[33], G.Damgaard[29], A.Daum[16], P.D.Dauncey[38], M.Davenport[8], W.Da Silva[23], C.Defoix[7], G.Della Ricca[47], P.Delpierre[27], N.Demaria[35], A.De Angelis[8], H.De Boeck[2], W.De Boer[16], S.De Brabandere[2], C.De Clercq[2], M.D.M.De Fez Laso[50], C.De La Vaissiere[23], B.De Lotto[47], A.De Min[28], L.De Paula[48], C.De Saint-Jean[40], H.Dijkstra[8], L.Di Ciaccio[39], F.Djama[9], J.Dolbeau[7], M.Donszelmann[8], K.Doroba[52], M.Dracos[9], J.Drees[53], K.-A.Drees[53], M.Dris[32], Y.Dufour[7], F.Dupont[13], D.Edsall[1], R.Ehret[16], T.Ekelof[49], G.Ekspong[45], M.Elsing[53], J-P.Engel[9], N.Ershaidat[23], M.Espirito Santo[21], D.Fassouliotis[32], M.Feindt[8], A.Fenyuk[43], A.Ferrer[50], T.A.Filippas[32], A.Firestone[1], H.Foeth[8], E.Fokitis[32], F.Fontanelli[12], F.Formenti[8], J-L.Fousset[27], B.Franek[38], P.Frenkiel[7], D.C.Fries[16], A.G.Frodesen[4], R.Fruhwirth[51], F.Fulda-Quenzer[19], H.Furstenau[8], J.Fuster[8], D.Gamba[46], M.Gandelman[18], C.Garcia[50], J.Garcia[42], C.Gaspar[8], U.Gasparini[36], Ph.Gavillet[8], E.N.Gazis[32], D.Gele[9], J-P.Gerber[9], D.Gillespie[8], R.Gokieli[52], B.Golob[44], J.J.Gomez Y Cadenas[8], G.Gopal[38], L.Gorn[1], M.Gorski[52], V.Gracco[12], F.Grard[2], E.Graziani[41], G.Grosdidier[19], P.Gunnarsson[45], J.Guy[38], U.Haedinger[16], F.Hahn[53], M.Hahn[16], S.Hahn[53], S.Haider[31], Z.Hajduk[17], A.Hakansson[24], A.Hallgren[49], K.Hamacher[53], W.Hao[31], F.J.Harris[35], V.Hedberg[24], R.Henriques[21], J.J.Hernandez[50], J.A.Hernando[50], P.Herquet[2], H.Herr[8], T.L.Hessing[8], E.Higon[50], H.J.Hilke[8], T.S.Hill[1], S-O.Holmgren[45], P.J.Holt[35], D.Holthuizen[31], P.F.Honore[7], M.Houlden[22], J.Hrubec[51], K.Huet[2], K.Hultqvist[45], P.Ioannou[3], P-S.Iversen[4], J.N.Jackson[22], R.Jacobsson[45], P.Jalocha[17], R.Janik[6], G.Jarlskog[24], P.Jarry[40], B.Jean-Marie[19], E.K.Johansson[45], L.Jonsson[24], P.Juillot[9], M.Kaiser[16], G.Kalmus[38], F.Kapusta[23], M.Karlsson[45], E.Karvelas[10], S.Katsanevas[3], E.C.Katsoufis[32], R.Keranen[14], B.A.Khomenko[15], N.N.Khovanski[15], B.King[22], N.J.Kjaer[29], H.Klein[8], A.Klovning[4], P.Kluit[31], J.H.Koehne[16], B.Koene[31], P.Kokkinias[10], M.Koratzinos[8], K.Korcyl[17], V.Kostioukhine[43], C.Kourkoumelis[3], O.Kouznetsov[12], P.-H.Kramer[53], M.Krammer[51], C.Kreuter[16], J.Krolikowski[52], I.Kronkvist[24], Z.Krumstein[15], W.Krupinski[17], P.Kubinec[6], W.Kucewicz[17], K.Kulka[49], K.Kurvinen[14], C.Lacasta[50], I.Laktineh[25], C.Lambropoulos[10], J.W.Lamsa[1], L.Lanceri[47], P.Langefeld[53], V.Lapin[43], I.Last[22], J-P.Laugier[40], R.Lauhakangas[14], F.Ledroit[13], V.Lefebure[2], R.Leitner[30], Y.Lemoigne[40], J.Lemonne[2], G.Lenzen[53], V.Lepeltier[19], T.Lesiak[36], J.M.Levy[9], D.Liko[51], R.Lindner[53], A.Lipniacka[19], I.Lippi[36], B.Loerstad[24], M.Lokajicek[11], J.G.Loken[35], A.Lopez-Fernandez[8], M.A.Lopez Aguera[42], D.Loukas[10], J.J.Lozano[50], P.Lutz[40], L.Lyons[35], G.Maehlum[16], J.Maillard[7], A.Maio[21], A.Maltezos[10], V.Malychev[15], F.Mandl[51], J.Marco[42], B.Marechal[48], M.Margoni[36], J-C.Marin[8], C.Mariotti[41], A.Markou[10], T.Maron[53], C.Martinez-Rivero[42], F.Martinez-Vidal[50], S.Marti i Garcia[50], F.Matorras[42], C.Matteuzzi[28], G.Matthiae[39], M.Mazzucato[36], M.Mc Cubbin[8], R.Mc Kay[1], R.Mc Nulty[22], J.Medbo[49], C.Meroni[28], W.T.Meyer[1], M.Michelotto[36], E.Migliore[46], I.Mikulec[51], L.Mirabito[25], W.A.Mitaroff[51], U.Mjoernmark[24], T.Moa[45], R.Moeller[29], K.Moenig[8], M.R.Monge[12], P.Morettini[12], H.Mueller[16], W.J.Murray[38], B.Muryn[17], G.Myatt[35], F.Naraghi[13], F.L.Navarria[5], S.Navas[50], P.Negri[28], S.Nemecek[11], W.Neumann[53], N.Neumeister[51], R.Nicolaidou[3], B.S.Nielsen[29], V.Nikolaenko[25], P.Niss[45], A.Nomerotski[36], A.Normand[35], W.Oberschulte-Beckmann[16], V.Obraztsov[43], A.G.Olshevski[15], R.Orava[14], K.Osterberg[14], A.Ouraou[40], P.Paganini[19], M.Paganoni[28], P.Pages[9], R.Pain[23], H.Palka[17], Th.D.Papadopoulou[32], L.Pape[8], F.Parodi[12], A.Passeri[41], M.Pegoraro[36], J.Pennanen[14], L.Peralta[21], V.Perevozchikov[43], H.Pernegger[51], M.Pernicka[51], A.Perrotta[5], C.Petridou[47], A.Petrolini[12], H.T.Phillips[38], G.Piana[12], F.Pierre[40], M.Pimenta[21], S.Plaszczynski[19], O.Podobrin[16], M.E.Pol[18], G.Polok[17], P.Poropat[47], V.Pozdniakov[15], M.Prest[47], P.Privitera[39], A.Pullia[28], D.Radojicic[35], S.Ragazzi[28], H.Rahmani[32], J.Rames[11], P.N.Ratoff[20], A.L.Read[33], M.Reale[53], P.Rebecchi[19], N.G.Redaelli[28], M.Regler[51], D.Reid[8], P.B.Renton[35], L.K.Resvanis[3], F.Richard[19], J.Richardson[22], J.Ridky[11], G.Rinaudo[46], I.Ripp[40], A.Romero[46], I.Roncagliolo[12], P.Ronchese[36], L.Roos[13], E.I.Rosenberg[1], E.Rosso[8], P.Roudeau[19], T.Rovelli[5], W.Ruckstuhl[31], V.Ruhlmann-Kleider[40], A.Ruiz[42], H.Saarikko[14], Y.Sacquin[40], A.Sadovsky[15], G.Sajot[13], J.Salt[50], J.Sanchez[26], M.Sannino[12], H.Schneider[16], M.A.E.Schyns[53], G.Sciolla[46], F.Scuri[47], Y.Sedykh[15], A.M.Segar[35], A.Seitz[16], R.Sekulin[38], R.C.Shellard[37], I.Siccama[31], P.Siegrist[40], S.Simonetti[40], F.Simonetto[36], A.N.Sisakian[15], B.Sitar[6], T.B.Skaali[33], G.Smadja[25], N.Smirnov[43], O.Smirnova[15], G.R.Smith[38], R.Sosnowski[52], D.Souza-Santos[37], T.Spassov[21], E.Spiriti[41], S.Squarcia[12], H.Staeck[53], C.Stanescu[41], S.Stapnes[33], I.Stavitski[36], G.Stavropoulos[10], K.Stepaniak[52], F.Stichelbaut[8], A.Stocchi[19], J.Strauss[51], R.Strub[9], B.Stugu[4],

M.Szczekowski[52], M.Szeptycka[52], T.Tabarelli[28], O.Tchikilev[43], G.E.Theodosiou[10], A.Tilquin[27], J.Timmermans[31], L.G.Tkatchev[15], T.Todorov[9], D.Z.Toet[31], A.Tomaradze[2], B.Tome[21], E.Torassa[46], L.Tortora[41], G.Transtromer[24], D.Treille[8], W.Trischuk[8], G.Tristram[7], A.Trombini[19], C.Troncon[28], A.Tsirou[8], M-L.Turluer[40], T.Tuuva[14], I.A.Tyapkin[23], M.Tyndel[38], S.Tzamarias[22], B.Ueberschaer[53], S.Ueberschaer[53], O.Ullaland[8], V.Uvarov[43], G.Valenti[5], E.Vallazza[8], J.A.Valls Ferrer[50], G.W.Van Apeldoorn[31], P.Van Dam[31], W.K.Van Doninck[2], J.Van Eldik[31], G.Vegni[28], L.Ventura[36], W.Venus[38], F.Verbeure[2], M.Verlato[36], L.S.Vertogradov[15], D.Vilanova[40], P.Vincent[25], L.Vitale[47], E.Vlasov[43], A.S.Vodopyanov[15], M.Voutilainen[14], V.Vrba[11], H.Wahlen[53], C.Walck[45], F.Waldner[47], A.Wehr[53], M.Weierstall[53], P.Weilhammer[8], A.M.Wetherell[8], D.Wicke[53], J.H.Wickens[2], M.Wielers[16], G.R.Wilkinson[35], W.S.C.Williams[35], M.Winter[9], M.Witek[8], G.Wormser[19], K.Woschnagg[49], K.Yip[35], O.Yushchenko[43], F.Zach[25], A.Zaitsev[43], A.Zalewska[17], P.Zalewski[52], D.Zavrtanik[44], E.Zevgolatakos[10], N.I.Zimin[15], M.Zito[40], D.Zontar[44], R.Zuberi[35], G.C.Zucchelli[45], G.Zumerle[36]

[1] Ames Laboratory and Department of Physics, Iowa State University, Ames IA 50011, USA
[2] Physics Department, Univ. Instelling Antwerpen, Universiteitsplein 1, B-2610 Wilrijk, Belgium
and IIHE, ULB-VUB, Pleinlaan 2, B-1050 Brussels, Belgium
and Faculté des Sciences, Univ. de l'Etat Mons, Av. Maistriau 19, B-7000 Mons, Belgium
[3] Physics Laboratory, University of Athens, Solonos Str. 104, GR-10680 Athens, Greece
[4] Department of Physics, University of Bergen, Allégaten 55, N-5007 Bergen, Norway
[5] Dipartimento di Fisica, Università di Bologna and INFN, Via Irnerio 46, I-40126 Bologna, Italy
[6] Comenius University, Faculty of Mathematics and Physics, Mlynska Dolina, SK-84215 Bratislava, Slovakia
[7] Collège de France, Lab. de Physique Corpusculaire, IN2P3-CNRS, F-75231 Paris Cedex 05, France
[8] CERN, CH-1211 Geneva 23, Switzerland
[9] Centre de Recherche Nucléaire, IN2P3 - CNRS/ULP - BP20, F-67037 Strasbourg Cedex, France
[10] Institute of Nuclear Physics, N.C.S.R. Demokritos, P.O. Box 60228, GR-15310 Athens, Greece
[11] FZU, Inst. of Physics of the C.A.S. High Energy Physics Division, Na Slovance 2, 180 40, Praha 8, Czech Republic
[12] Dipartimento di Fisica, Università di Genova and INFN, Via Dodecaneso 33, I-16146 Genova, Italy
[13] Institut des Sciences Nucléaires, IN2P3-CNRS, Université de Grenoble 1, F-38026 Grenoble Cedex, France
[14] Research Institute for High Energy Physics, SEFT, P.O. Box 9, FIN-00014 Helsinki, Finland
[15] Joint Institute for Nuclear Research, Dubna, Head Post Office, P.O. Box 79, 101 000 Moscow, Russian Federation
[16] Institut für Experimentelle Kernphysik, Universität Karlsruhe, Postfach 6980, D-76128 Karlsruhe, Germany
[17] High Energy Physics Laboratory, Institute of Nuclear Physics, Ul. Kawiory 26a, PL-30055 Krakow 30, Poland
[18] Centro Brasileiro de Pesquisas Físicas, rua Xavier Sigaud 150, BR-22290 Rio de Janeiro, Brazil
[19] Université de Paris-Sud, Lab. de l'Accélérateur Linéaire, IN2P3-CNRS, Bat 200, F-91405 Orsay Cedex, France
[20] School of Physics and Materials, University of Lancaster, Lancaster LA1 4YB, UK
[21] LIP, IST, FCUL - Av. Elias Garcia, 14-1^{o}, P-1000 Lisboa Codex, Portugal
[22] Department of Physics, University of Liverpool, P.O. Box 147, Liverpool L69 3BX, UK
[23] LPNHE, IN2P3-CNRS, Universités Paris VI et VII, Tour 33 (RdC), 4 place Jussieu, F-75252 Paris Cedex 05, France
[24] Department of Physics, University of Lund, Sölvegatan 14, S-22363 Lund, Sweden
[25] Université Claude Bernard de Lyon, IPNL, IN2P3-CNRS, F-69622 Villeurbanne Cedex, France
[26] Universidad Complutense, Avda. Complutense s/n, E-28040 Madrid, Spain
[27] Univ. d'Aix - Marseille II - CPP, IN2P3-CNRS, F-13288 Marseille Cedex 09, France
[28] Dipartimento di Fisica, Università di Milano and INFN, Via Celoria 16, I-20133 Milan, Italy
[29] Niels Bohr Institute, Blegdamsvej 17, DK-2100 Copenhagen 0, Denmark
[30] NC, Nuclear Centre of MFF, Charles University, Areal MFF, V Holesovickach 2, 180 00, Praha 8, Czech Republic
[31] NIKHEF-H, Postbus 41882, NL-1009 DB Amsterdam, The Netherlands
[32] National Technical University, Physics Department, Zografou Campus, GR-15773 Athens, Greece
[33] Physics Department, University of Oslo, Blindern, N-1000 Oslo 3, Norway
[34] Dpto. Fisica, Univ. Oviedo, C/P. Pérez Casas, S/N-33006 Oviedo, Spain
[35] Department of Physics, University of Oxford, Keble Road, Oxford OX1 3RH, UK
[36] Dipartimento di Fisica, Università di Padova and INFN, Via Marzolo 8, I-35131 Padua, Italy
[37] Depto. de Fisica, Pontificia Univ. Católica, C.P. 38071 RJ-22453 Rio de Janeiro, Brazil
[38] Rutherford Appleton Laboratory, Chilton, Didcot OX11 OQX, UK
[39] Dipartimento di Fisica, Università di Roma II and INFN, Tor Vergata, I-00173 Rome, Italy
[40] Centre d'Etude de Saclay, DSM/DAPNIA, F-91191 Gif-sur-Yvette Cedex, France
[41] Istituto Superiore di Sanità, Ist. Naz. di Fisica Nucl. (INFN), Viale Regina Elena 299, I-00161 Rome, Italy
[42] C.E.A.F.M., C.S.I.C. - Univ. Cantabria, Avda. los Castros, S/N-39006 Santander, Spain, (CICYT-AEN93-0832)
[43] Inst. for High Energy Physics, Serpukov P.O. Box 35, Protvino, (Moscow Region), Russian Federation
[44] J. Stefan Institute and Department of Physics, University of Ljubljana, Jamova 39, SI-61000 Ljubljana, Slovenia
[45] Fysikum, Stockholm University, Box 6730, S-113 85 Stockholm, Sweden
[46] Dipartimento di Fisica Sperimentale, Università di Torino and INFN, Via P. Giuria 1, I-10125 Turin, Italy
[47] Dipartimento di Fisica, Università di Trieste and INFN, Via A. Valerio 2, I-34127 Trieste, Italy
and Istituto di Fisica, Università di Udine, I-33100 Udine, Italy
[48] Univ. Federal do Rio de Janeiro, C.P. 68528 Cidade Univ., Ilha do Fundão BR-21945-970 Rio de Janeiro, Brazil
[49] Department of Radiation Sciences, University of Uppsala, P.O. Box 535, S-751 21 Uppsala, Sweden
[50] IFIC, Valencia-CSIC, and D.F.A.M.N., U. de Valencia, Avda. Dr. Moliner 50, E-46100 Burjassot (Valencia), Spain
[51] Institut für Hochenergiephysik, Österr. Akad. d. Wissensch., Nikolsdorfergasse 18, A-1050 Vienna, Austria
[52] Inst. Nuclear Studies and University of Warsaw, Ul. Hoza 69, PL-00681 Warsaw, Poland
[53] Fachbereich Physik, University of Wuppertal, Postfach 100 127, D-42097 Wuppertal 1, Germany

1 Introduction

A precise measurement of the relative decay width of the Z into b-hadrons, $R_b = \frac{\Gamma_{b\bar{b}}}{\Gamma_{had}}$, is an important test of the Standard Model which predicts a value that is dependent on the top mass m_t [1] via weak vertex corrections. To a large extent the ratio is independent of other corrections such as QED or QCD corrections or electroweak corrections to the Z-propagator.

This paper presents four measurements of R_b using data taken in 1991-1992 with the DELPHI detector at LEP based on events with one or two identified leptons and on tagging techniques using a high resolution silicon micro-vertex detector. Using the single and double lepton events R_b is determined together with the semileptonic branching ratio $BR(b \to l)$ and other properties of $Z \to b\bar{b}$ and $Z \to c\bar{c}$ decays. The fraction of events initiated by $Z \to b\bar{b}$ in a sample containing a lepton with a high transverse momentum is derived. The highest precision on R_b is obtained from analyses using lifetime tagging techniques which are either used alone comparing single and double tag rates or combined with the lepton tag.

2 The DELPHI Detector

The DELPHI detector has been described in detail in ref. [2]. Only the details most relevant to this analysis are mentioned here.

In the barrel region, the charged particle tracks are measured by a set of cylindrical tracking detectors whose axes are parallel to the 1.2 T solenoidal magnetic field and to the beam direction. The time projection chamber (TPC) is the main tracking device. The TPC is a cylinder with a length of 3 m, an inner radius of 30 cm and an outer radius of 122 cm. Between polar angles, θ, of 39° and 141° with respect to the beam direction, tracks are reconstructed using up to 16 space points. Outside this region (21° to 39° and 141° to 159°), tracks can be reconstructed using at least 4 space points.

Additional precise $R\Phi$ measurements, in the plane perpendicular to the magnetic field, are provided at larger and smaller radii by the Outer and Inner detectors respectively. The Outer Detector (OD) has five layers of drift cells at radii between 198 and 206 cm and covers polar angles from 42° to 138°. The Inner Detector (ID) is a cylindrical drift chamber having inner radius of 12 cm and outer radius of 28 cm. It covers polar angles between 29° and 151° . It contains a jet chamber section providing 24 $R\Phi$ coordinates surrounded by five layers of proportional chambers providing both $R\Phi$ and longitudinal z coordinates.

The micro-vertex detector (VD) is located between the LEP beam pipe and the ID [3]. It consists of three concentric layers of silicon microstrip detectors placed at radii of 6.3, 9 and 11 cm from the interaction region. For all layers the microstrip detectors provide hits in the $R\Phi$-plane with a measured intrinsic resolution of about 8 μm. The polar angle coverage for charged particles hitting all three layers of the detector is 42.5° to 137.5°.

The barrel electromagnetic calorimeter, HPC, covers the polar angles between 42° and 138°. It is a gas-sampling device which provides complete three dimensional charge information in the same way as a time projection chamber. Each shower is sampled nine times in its longitudinal development. Along the drift direction, parallel to the DELPHI magnetic field, the shower is sampled every 3.5 mm ; in the plane perpendicular to the drift the charge is collected by cathode pads of variable size, ranging from 2.3 cm in the inner part of the detector to 7 cm in the outer layers. The excellent granularity allows

good separation between close particles in three dimensions and hence good electron identification even inside jets.

In the forward region the tracking is complemented by two sets of planar drift chambers (FCA and FCB) placed at distances of ± 165 cm and ± 275 cm from the interaction point. A lead glass calorimeter (EMF) is used to reconstruct electromagnetic energy in the forward region.

Muon identification in the barrel region is based on a set of muon chambers (MUB), covering polar angles between 53° and 127°. It consists of six active planes of drift chambers, two inside the return yoke of the magnet after 90 cm of iron (inner layer) and four outside after a further 20 cm of iron (outer and peripheral layers). The inner and outer modules have similar azimuthal coverage. The gaps in azimuth between adjacent modules are covered by the peripheral modules. Therefore a muon traverses typically either two inner layer chambers and two outer layer chambers, or just two peripheral layer chambers. Each chamber measures the $R\Phi$ coordinate to 2–3 mm. Measuring $R\Phi$ in both the inner layer and the outer or peripheral layer determines the azimuthal angle of muon candidates leaving the return yoke within about $\pm 1°$. These errors are much smaller than the effects of multiple scattering on muons traversing the iron.

In the forward region the muon identification is done using two sets of planar drift chambers (MUF) covering the angular region between 11° and 45°. The first set is placed behind 85 cm of iron and the second one behind an additional 20 cm. Each set consists of two orthogonal layers of drift chambers where the anode is read out directly and the cathode via a delay line to measure the coordinate along the wire. The resolution in both coordinates is about 4 mm.

3 Event Selection

The decays of the Z to hadrons were selected by requiring:

- at least 7 reconstructed charged particles (with criteria described below),
- the summed energy of the charged particles had to be larger than 15 % of the centre of mass energy and at least 3 % of it in both the forward and backward hemispheres with respect to the beam axis.

Charged particles were accepted if:

- their polar angle was between 20° and 160°,
- their track length was larger than 30 cm,
- their impact parameter relative to the interaction point was less than 2.5 cm in the plane perpendicular to the beam direction and less than 10 cm along the beam direction,
- their momentum was larger than 200 MeV/c with relative error less than 100%.

Neutral particles detected in the HPC were required to have measured energy larger than 700 MeV, those detected in the EMF larger than 400 MeV.

With these criteria, the efficiency for finding simulated $q\bar{q}$ events was about 95%. All sources of background have been found to be below 0.1%. No significant differences in the acceptance between different flavours have been found.

About 700000 (200000) hadronic Z decays have been selected from the 1992 (1991) data sample where the exact numbers vary between the different analyses due to different requirements on the detector availability. A slightly larger sample of $Z \to q\bar{q}$ events has been simulated using the Lund parton shower Monte Carlo JETSET 7.3 [4] with parameters optimized by DELPHI and the DELPHI detector simulation [5]. In addition dedicated samples of $Z \to b\bar{b}$ events and $Z \to c\bar{c}$ events and events containing a semileptonic B or D decay have been generated. The simulated events have been passed through the same analysis chain as the real ones.

4 Lepton Analysis

4.1 Data Analysis

For each event the thrust axis was calculated from all the charged and neutral particles selected as above. Only the events with

$$|\cos\theta_{thrust}| < 0.95$$

were used for the following analysis. Requiring, in addition, that all subdetectors needed for this analysis were fully functional a total of 590,000 (170,000) hadronic events were selected from the 1992 (1991) data samples. Jets were formed from the charged and neutral particles using the JADE algorithm [6] with $Y_{cut}^{min} = 0.01$. The transverse momentum of the lepton, (p_t), was determined relative to the direction of the jet excluding the lepton itself.

For the 1992 data all leptons with momentum p between 3 GeV/c and 30 GeV/c, transverse momentum between 0.4 GeV/c and 4 GeV/c, were used. For the 1991 data, where the understanding of the background was not as good, the momentum threshold was raised to 4 GeV/c. From the 1992 data sample about 56000 single leptons and 2500 lepton pairs have been selected. For 1991 the corresponding numbers were 12000 and 500.

4.1.1 Muon Identification

To identify a charged particle with momentum greater than 3 GeV/c as a muon candidate, its track was extrapolated to each of the layers of the muon chambers and a χ^2 was calculated for individual hits taking into account multiple scattering in the material and the propagation of track reconstruction errors.

Ambiguities with muon chamber hits associated to more than one extrapolated track were resolved by selecting the track with the smallest mean χ^2. The charged particle was then tagged as a muon if the χ^2 was sufficiently small.

To exclude regions with poor geometrical acceptance the charged particle was accepted if the polar angle, θ_μ, was within one of the following intervals

$$0.03 < |\cos\theta_\mu| < 0.62$$

$$0.68 < |\cos\theta_\mu| < 0.90,$$

which defined the barrel and the forward region, respectively. In $Z \to \mu^+\mu^-$ events the tagging efficiencies for a single muon in the data were determined to be 0.83 ± 0.01 in

the barrel region and 0.89 ± 0.01 in the forward region, in good agreement with the predictions of the simulation. For muons in hadronic jets, the efficiency was found to be 0.76 ± 0.01 in the barrel region and 0.81 ± 0.02 in the forward region using the simulation. The hadron misidentification probability was determined from data using pions from K_s° and τ decays to be 0.007 ± 0.001.

4.1.2 Electron Identification

Charged particles with momenta greater than 3 GeV/c and within the good acceptance region of the HPC ($0.03 < |\cos\theta_e| < 0.70$) were accepted as electron candidates on the basis of the information from the HPC and the TPC. Tracks were extrapolated to the HPC where showers were associated to them. Probabilities of the charged particle being an electron were computed by comparison of track and shower parameters (momentum-energy and position) and the longitudinal shower development along the 9 layers of the calorimeter. In addition the ionization energy loss in the TPC was required to be compatible with that expected for an electron.

The efficiency of tagging an electron was measured in the data over the full momentum range by means of a set of isolated electrons extracted from selected τ decays and Bhabha events in which one hard photon was emitted. The efficiency increased slightly with momentum for small momenta, reaching a plateau of $\epsilon^{tag}_{electrons} = 0.625 \pm 0.006$ above 5 GeV/c. The efficiency was then compared to that of the simulated event samples of the same size. The ratio of the experimental efficiency to the simulated one was 0.92 ± 0.02. This factor was found to be independent of momentum. It was then applied to the sample of electrons from the simulated $q\overline{q}$ events, assuming it applied to non-isolated electrons as well. A systematic error of $\pm$ 4% was added to allow for uncertainties in this procedure.

The probability of tagging a hadron as an electron was measured in the data as a function of p and p_t, by studying the HPC tags for a sample of particles whose ionization in the TPC was incompatible with that of an electron [7]. The results were used to correct the distributions of the background in the simulation. The probability of a fake tag depended strongly on the values of p and p_t. The average value in the region considered was $\epsilon^{mistag}_{hadrons} = (5.91 \pm 0.07) \times 10^{-3}$. The quoted error is statistical only. A relative systematic uncertainty of $\pm$20% was estimated for this measurement.

To reduce the contamination from electrons from photon conversions, electron candidates were removed if they were consistent with coming from a secondary vertex with an oppositely charged particle and with the two-particle combination compatible with carrying no transverse momentum to the direction from the primary to the secondary vertex.

The residual number of conversion electrons was found from the simulation to be a factor 1.4 ± 0.2 less than in data (see [7]), and was corrected for. Only about 3% of the electrons from b-quark decay were removed as photon conversions in the simulation. This efficiency was checked by applying the algorithm to the muon candidates both in the data and in the simulation: consistent results were found.

4.1.3 Measurement of the Lepton Background

Apart from the tests described above, another measurement of the background in $q\overline{q}$ events was performed. The basic idea was that all the leptons found in $u\bar{u}$,$d\bar{d}$, $s\bar{s}$ events originate from background sources. If a sample of events enriched in those light quarks were provided both in the data and in the simulation, it would then be possible to measure the experimental misidentification probability with respect to the predicted one.

Light quark events were selected by means of the lifetime tag described in section 5 where it is used the opposite way to provide a set of events enriched in b-hadrons. By requiring that the probability for all the tracks in a hemisphere to come from the primary vertex be greater than 80 %, a set of events was produced containing only 0.079 ± 0.005 (0.147 ± 0.034) of $b\bar{b}$ ($c\bar{c}$) pairs. The fractions of charged particles in the sample which were tagged as leptons were compared in the data and in the simulation, separately for muons and electrons. A fit was performed to the p,p_t two dimensional distribution of the leptons, similar to the one described in section 4.3.2. This also allowed a check to be made on the goodness of the description of the background in the simulation as a function of p and p_t.

The only free parameter in the muon fit was the ratio of the hadron misidentification probability as muons in the data to that in the simulation. The results of the fit showed this to be $0.99 \pm 0.05(stat.) \pm 0.11(syst.)$.The systematic error is dominated by the uncertainty on the amount of $c\bar{c}$ events in the sample, whereas the uncertainties due to b,c semileptonic decays (see below) turned out to be negligible. The χ^2 was 15.9 for 16 degrees of freedom. By combining this measurement with the one from the K°_s and τ samples described above, an overall relative error of $\pm 10\%$ was obtained on the muon misidentification probability.

In the electron sample, both the fraction of pions misidentified and the relative amount of electrons from conversions were left free. The ratio of the efficiencies in the data to the simulation were respectively $f_{\pi\to e} = 0.94 \pm 0.14$ and $f_\gamma = 1.56 \pm 0.29$, with $\chi^2/n.d.f = 14.02/14$. Each fraction was measured with poor statistical precision, but there was an anticorrelation between the two parameters, $\rho = -0.897$. For this reason, it was decided in the following analysis to fix the amount of fake hadrons to the value in the tuned simulation and to obtain the fraction of electrons from conversion from the fit to the single and di-lepton distributions described in section 4.3.2.

4.2 The Simulated Lepton Sample

4.2.1 Assumptions on Models and Branching Ratios

Several models have been proposed to describe the semileptonic decays of heavy flavour hadrons. In this analysis the following ones were used. The form factor model by Isgur et al. [8], henceforth called the IGSW model, calculates exclusive semileptonic b decays. In principle it contains no free parameters. However CLEO finds that the model describes their data only if the $\frac{D^{**}}{D+D^*+D^{**}}$ ratio is set to 32% instead of 11% as calculated in the model [9]. This modification (denoted as IGSW**) was then used to analyse our data. The model of Altarelli et al. [10] (ACCMM) is a spectator model refined by QCD corrections. It contains two free parameters, the Fermi motion and the mass of the produced quark. These parameters were measured by CLEO [9] for b decays. In the same fits the rate of charmless b semileptonic decays ($b \to u$) was also measured. That value was assumed for the present analysis, allowing for $\pm 50\%$ systematic uncertainty. At CLEO energies, only B^0_d and $B^\pm$ mesons are produced, whereas at LEP energies B^0_s and b baryons have also been observed. It was assumed that the lepton spectra for all b-hadrons are identical. Since the IGSW** and ACCMM model describe the CLEO data equally well, the mean value of the results with these two models was used as the central value in the following analysis and half the difference as an estimate of the uncertainty due to the model dependence. The results using IGSW are given only for comparison and are not further taken into account.

Charm hadron semileptonic decays were described by means of the ACCMM model, where the mass and the Fermi momentum of the produced strange quark were obtained from a combined fit to the data from DELCO and MARK II [11]. The three sets of parameters (m_s, p_f), as obtained from the fit, were used (set 1: $m_s = 0.001$ GeV/c^2, $p_f = 0.467$ GeV/c, set 2: $m_s = 0.001$ GeV/c^2, $p_f = 0.353$ GeV/c, set 3: $m_s = 0.153$ GeV/c^2, $p_f = 0.467$ GeV/c).

For $b \to c \to l$ decays the D momentum spectra obtained by CLEO [12] were folded with the spectra used for the $c \to l$ decays [11]. The uncertainty in the $B \to D$ spectra turned out to be negligible in the description of the lepton spectra so that only the uncertainty on $c \to l$ was taken into account.

The $b \to \tau$ decay rate was taken as $(4.08 \pm 0.74)\%$ as measured by ALEPH [13]. The $b \to \bar{c} \to l$ decay rate was assumed to be $(1.3 \pm 0.5)\%$ [11]. The branching ratio $c \to l$ has been measured by ARGUS just below the $b\bar{b}$-threshold to be $(9.5 \pm 0.9)\%$ [14]. For the present analysis this number was combined with the values measured by PEP and PETRA quoted in [14] where for all measurements above the $b\bar{b}$-threshold a common systematic error of 0.3% for the treatment of the $b \to c \to l$ contribution was assumed. The obtained average value was $(9.8 \pm 0.5)\%$. The branching ratio $b \to J/\psi \to l\bar{l}$ was assumed to be $(0.07 \pm 0.02)\%$ [15].

For the charm fragmentation DELPHI has measured the mean momentum of D mesons to be $< x >_c = 0.487 \pm 0.016$ [16]. Using $\Lambda_{QCD} = 255$ MeV this corresponds to a parameter $\epsilon_c = 0.076^{+0.029}_{-0.020}$ in the Peterson fragmentation function [17]. This value was used in our analysis.

The Peterson fragmentation function was assumed for b quarks. To evaluate the systematic uncertainties the fits were repeated with the functions of Collins and Spiller [18] and Kartvelishvili et al [19].

4.2.2 Simulated Samples

As reference spectra for the different sources of simulated leptons, samples were used that were processed through the same analysis chain as the data as descibed in section 3. The b semileptonic decays to electrons and muons were simulated using the IGSW** model. The model of Bauer et al. [20], which takes into account the finite mass of the produced lepton, was used for the B decays into τ's. For D decays the branching ratios were adjusted to be better in agreement with measured values [15]; the branching ratios for the decays to neutral pions, when not measured, were obtained imposing isospin invariance. To obtain the reference spectra with alternative models, events were reweighted according to the decay model considered. The weight was computed on the basis of the lepton momentum in the B(D) rest frame.

In this analysis the statistical precision of the measurements is mainly related to the number of events where two leptons were found. The main contributions are events where either both tagged particles are true leptons from the classes $b \to l$, $b \to c \to l$ and $c \to l$ or one particle is from these classes and the other is a lepton from a different source or a misidentified hadron. Therefore, besides the normal $Z \to q\bar{q}$ events extra samples were simulated with events containing at least one lepton from b or c decay. Table 1 details the channels simulated, expressed as an equivalent number of hadronic Z decays.

channel	equivalent hadronic Z decays $\times 10^6$
$q\bar{q}$	1.1
$b \to e$,$b \to J/\Psi \to e$	3.3
$b \to c \to e$,$b \to \tau \to e$	1.4
$c \to e$	4.3
$b \to \mu$,$b \to J/\Psi \to \mu$	4.6
$b \to c \to \mu$,$b \to \tau \to \mu$	3.2
$c \to \mu$	4.6

Table 1: Simulation statistics used

4.3 Determination of $\Gamma_{b\bar{b}}$ and $BR(b \to l)$

4.3.1 Classification of Lepton Candidates

Lepton candidates were classified according to their different origin as follows:

a) direct b-decay:
$b \to l^- + X$,

b) "right sign" cascade decays:
$b \to \tau^- + X \to l^- + X$,
$b \to \bar{c} + X \to l^- + X$,

c) "wrong sign" cascade decays:
$b \to c + X \to l^+ + X$,

d) direct c-decay
$c \to l^+ + X$,
$c \to \tau^+ + X \to l^+ + X$,

e) prompt leptons from J/Ψ decays or from b,c decays, where the $c\bar{c}$ ($b\bar{b}$) pair is produced by gluon splitting,

f) misidentified or decaying hadrons.

The above classes gave both electrons and muons. There was an additional class of electrons from photon conversions and Dalitz decays since the rejection efficiency for such electrons was found to be only 75%.

The lepton candidates in the simulation were separated into these classes and reference (p,p_t) distributions were obtained for the single leptons. The p and p_t distributions for muons and electrons are shown in figures 1 and 2 for the 1992 sample. The simulation spectra are reweighted to the results of the fit described below.

Di-lepton events were separated, for both the data and the simulated samples, into six categories depending on whether the two lepton candidates have the same or opposite charge and on which combination of lepton species (ee, $e\mu$, $\mu\mu$) they belonged to. Lepton pairs were used where the two leptons were coming from different jets, while lepton pairs coming from the same jet were omitted from the fit. Including them would give only a marginal gain in statistical precision but would then introduce some additional

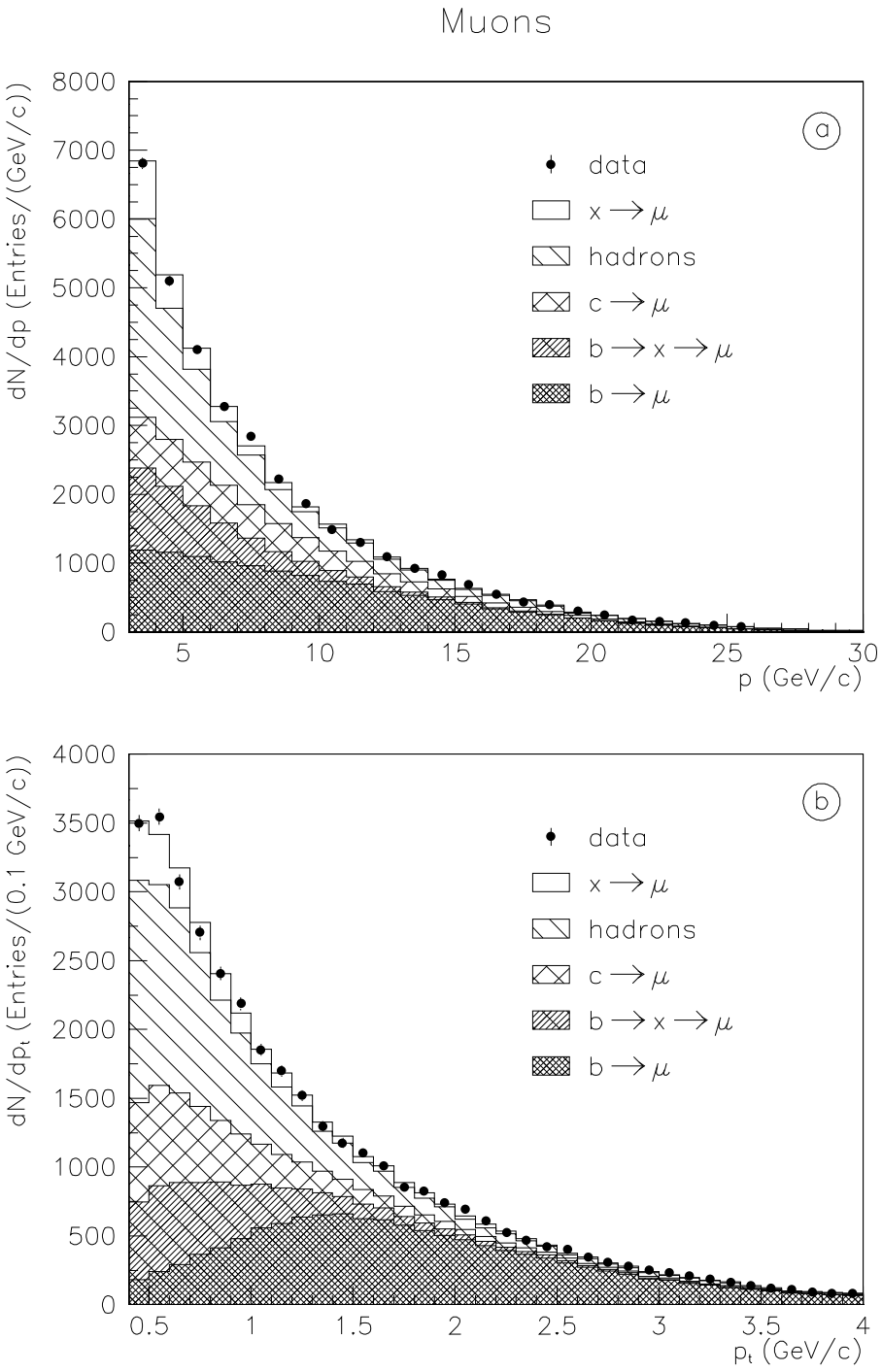

Figure 1: Momentum (a) and transverse momentum(b) distributions for muons for data and simulation. The statistical errors of the simulated samples are included in the error bars shown for the data.

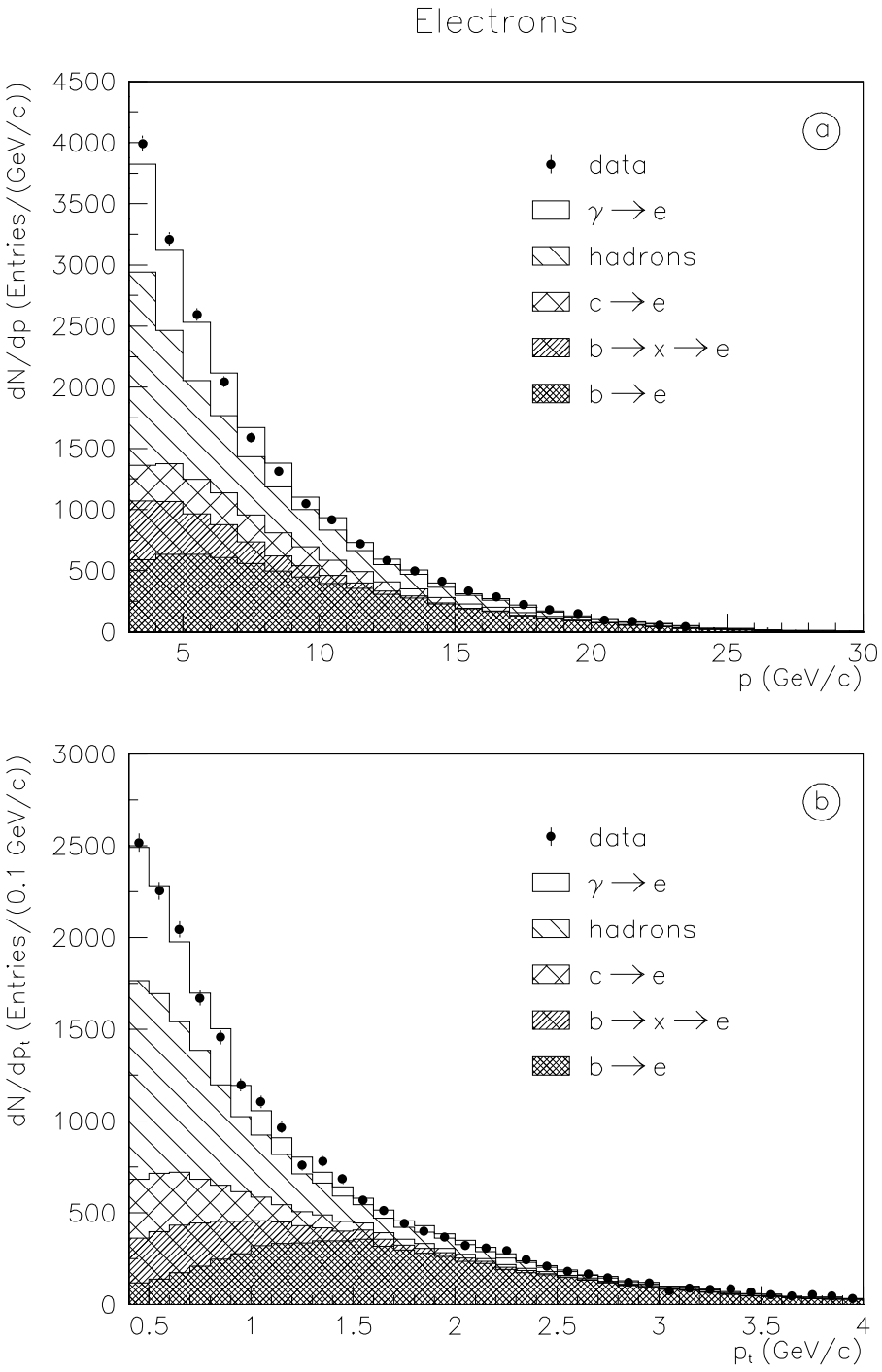

Figure 2: Momentum (a) and transverse momentum(b) distributions for electrons for data and simulation. The statistical errors of the simulated samples are included in the error bars shown for the data.

systematic uncertainties, such as those studied in detail by OPAL [21]. In each category the simulated events were separated into groups consisting of allowed combinations of the above mentioned classes. To guarantee a reasonable number of events in each bin, the p and p_t of each lepton in the pair were combined to form one variable, the combined momentum, p_c, defined as $p_c = \sqrt{p_t^2 + \frac{p^2}{100}}$. Two-dimensional reference distributions were obtained for the chosen combinations in the variables (p_c^{min}, p_c^{max}), where p_c^{min}, (p_c^{max}) refers to the smaller (bigger) of the two combined momenta.

4.3.2 Fit Procedure

The simulated single and dilepton distributions were fitted to the data with a binned maximum likelihood expression assuming Poisson errors and including the effect of finite simulation statistics [22]. The following parameters were left free to vary in the fit:

- The fraction of $b\bar{b}$ events R_b,
- the semileptonic branching ratio of the b-hadrons $BR(b \to l)$ $(= bl)$,
- the cascade branching ratio $BR(b \to c \to l)$ $(= bcl)$,
- the fraction of $c\bar{c}$ events R_c,
- the average mixing parameter χ_b,
- the Peterson fragmentation parameter ϵ_b which was always converted into the mean energy of b-flavoured hadrons $\langle x_E \rangle$.

Apart from these physical parameters the γ conversion rate and the electron identification efficiency were left free, but to the likelihood function a constraint on these parameters from the independent measurements discussed in section 4.1.2 was added. In the fit χ_b was included because the separation of same sign and opposite sign pairs improves the precision on all parameters. However it does not supersede our value given in a separate publication [23] which is more precise.

The 1991 and 1992 data samples have been fitted separately and the results combined afterwards using the full covariance matrix.

4.3.3 Results and Systematic Uncertainties

Using the average of the ACCMM and the IGSW** models the following results have been obtained:
1991 data:

$$\begin{aligned} R_b &= 0.2063 \pm 0.020, \\ BR(b \to l) &= (11.22 \pm 1.00)\%, \\ BR(b \to c \to l) &= (7.35 \pm 1.15)\%, \\ R_c &= 0.1332 \pm 0.019, \\ \langle x_E \rangle &= 0.7159 \pm 0.0077, \\ \chi_b &= 0.158 \pm 0.042; \end{aligned}$$

1992 data:

$$\begin{aligned} R_b &= 0.2165 \pm 0.010, \\ BR(b \to l) &= (11.48 \pm 0.50)\%, \\ BR(b \to c \to l) &= (7.37 \pm 0.53)\%, \\ R_c &= 0.1684 \pm 0.0095, \\ \langle x_E \rangle &= 0.6950 \pm 0.0053, \\ \chi_b &= 0.153 \pm 0.022; \end{aligned}$$

Combined data:

$$\begin{aligned} R_b &= 0.2145 \pm 0.0089, \\ BR(b \to l) &= (11.41 \pm 0.45)\%, \\ BR(b \to c \to l) &= (7.36 \pm 0.49)\%, \\ R_c &= 0.1623 \pm 0.0085, \\ \langle x_E \rangle &= 0.7020 \pm 0.0044, \\ \chi_b &= 0.154 \pm 0.020, \end{aligned}$$

where the errors are statistical only. Table 2 gives the numbers for the different b decay models. The electron efficiency and gamma conversion rate were reproduced by the fit to within 1 and 1.5 standard deviations respectively.

model	R_b	bl	bcl	R_c	$\langle x_E \rangle$	χ_b
ACCMM	0.2145	11.21	7.70	0.1625	0.6985	0.150
IGSW**	0.2146	11.61	7.01	0.1621	0.7055	0.158
IGSW	0.2138	11.03	8.14	0.1639	0.6883	0.147

Table 2: Results using different b decay models.

To test the quality of the fit a χ^2 test was performed after the fit. For the 1992 data the global probability was 51%. For 1991 the statistics was too low in the double lepton samples to perform a reasonable test; however for the single muons (electrons) the probability was 51% (3%).

To evaluate the experimental systematic errors the following sources of errors were considered:

- the electron misidentification probability was varied by $\pm 20\%$,
- the muon identification efficiency was varied by $\pm 2\%$,
- the muon misidentification probability was varied by $\pm 10\%$.

The muon identification efficiencies were measured separately for the the barrel and each end-cap muon chamber, and were varied separately to evaluate the systematic error. The experimental systematic errors are given in table 3. The correlation matrix for the

statistical error only and for the total experimental error is shown in table 4. For the combinations of the 1991 and 1992 analyses the systematical errors due to backgrounds were assumed to be fully correlated whereas the error on the muon identification efficiency was assumed to be uncorrelated because its measurement accuracy was dominated by the statistics.

	range	R_b	bl	bcl	R_c	$\langle x_E \rangle$	χ
μ background	$\pm 10\%$	∓ 0.0054	± 0.30	∓ 0.91	∓ 0.0160	∓ 0.0020	± 0.010
ϵ_μ endcaps	$\pm 2\%$	∓ 0.0004	∓ 0.03	∓ 0.04	∓ 0.0014	∓ 0.0002	0.
ϵ_μ barrel	$\pm 2\%$	± 0.0014	∓ 0.32	∓ 0.25	∓ 0.0038	± 0.0003	0.
e background	$\pm 20\%$	∓ 0.0029	± 0.24	± 0.05	∓ 0.0031	± 0.0003	∓ 0.003
total:		± 0.0063	± 0.50	± 0.95	± 0.0168	± 0.0021	± 0.010

Table 3: Summary of experimental systematic uncertainties.

	R_b	bl	bcl	R_c	$\langle x_E \rangle$	χ
R_b	1.00	-0.89	0.24	0.29	0.20	-0.25
bl	-0.95	1.00	-0.16	-0.23	-0.28	0.22
bcl	-0.38	0.29	1.00	0.69	0.42	-0.45
R_c	-0.42	0.37	-0.40	1.00	0.31	-0.29
$\langle x_E \rangle$	0.00	-0.15	0.18	-0.04	1.00	-0.13
χ	-0.09	0.11	-0.17	0.17	0.07	1.00

Table 4: Correlation matrix of statistical and experimental uncertainties. The numbers below the diagonal are for the statistical errors only, the numbers above the diagonal for the total experimental errors.

To obtain the systematic uncertainties due to the modelling of the decays the branching ratios derived for the models of section 4.2.1 were varied within the limits given there. The resulting systematic errors are given in table 5. The total uncertainty due to modelling and branching ratios was taken as the quadratic sum of all components in table 5 except for those from the c-quark decay model set 3. Instead the variations using c-quark decay model set 2 only were used and were taken to be symmetric. Table 6 gives the full correlation matrix including statistical and systematic effects in this analysis.

5 The Lifetime Analysis

5.1 Description of the Method and Tagging Technique

The method used for the measurement of R_b is based on the fact that b and $\bar{b}$ quarks from Z decays (and the corresponding heavy hadrons) are normally produced in opposite directions. On dividing such an event into 2 hemispheres (e.g. by the plane perpendicular to the thrust axis), each will, in general, contain one b-hadron.

If with some tag a pure b flavour sample can be selected in one hemisphere, it is possible to find the efficiency of this selection and the fraction of $b\bar{b}$ events in the initial sample in a model-independent way by comparing the number of selected single hemispheres with the number of events in which both hemispheres are selected.

	range	R_b	bl	bcl	R_c	$\langle x_E \rangle$	χ
b decay model	$^{IGSW**}_{ACCMM}$	± 0.0001	± 0.20	∓ 0.34	∓ 0.0002	± 0.0037	± 0.004
c decay model	set 2	$+0.0007$	-0.16	-0.03	$+0.0049$	$+0.0023$	-0.006
c decay model	set 3	$+0.0002$	$+0.11$	-0.05	$+0.0022$	-0.0012	-0.004
$BR(b \to u)$	$\pm 50\%$	0	0	∓ 0.03	± 0.0002	± 0.0016	∓ 0.004
$BR(c \to l)$	$\pm 5.1\%$	± 0.0014	∓ 0.06	∓ 0.04	∓ 0.0098	± 0.0002	∓ 0.002
$BR(b \to \bar{c} \to l)$	$\pm 40\%$	± 0.0003	± 0.01	∓ 0.33	± 0.0013	∓ 0.0002	± 0.003
$BR(b \to \tau)$	$\pm 18\%$	∓ 0.0002	∓ 0.03	∓ 0.13	∓ 0.0002	± 0.0008	± 0.001
$BR(b \to J/\psi \to l)$	$\pm 29\%$	± 0.0002	∓ 0.06	± 0.02	0	0	∓ 0.002
ϵ_c	$^{+0.029}_{-0.020}$	∓ 0.0015	± 0.17	∓ 0.28	± 0.0056	∓ 0.0002	± 0.003
b fragm. model	see Text	∓ 0.0008	± 0.11	∓ 0.03	± 0.0008	∓ 0.0053	∓ 0.002
total:		0.0023	0.34	0.57	0.0124	0.0071	0.011

Table 5: Summary of systematic uncertainties due to models and branching ratios. If a range is given in % it means a relative variation around the central value. For the total error the deviations using $c \to l$ (set 3) and the Kartvelishvili fragmentation function have been ignored and $c \to l$ (set 2) and the Collins and Spiller function have been taken as having symmetric errors.

	R_b	bl	bcl	R_c	$\langle x_E \rangle$	χ
R_b	1.00	-0.84	0.23	0.13	0.18	-0.25
bl	-0.84	1.00	-0.25	-0.03	-0.18	0.29
bcl	0.23	-0.25	1.00	0.49	0.09	-0.45
R_c	0.13	-0.03	0.49	1.00	0.05	-0.12
$\langle x_E \rangle$	0.18	-0.18	0.09	0.05	1.00	0.00
χ	-0.25	0.29	-0.45	-0.12	0.00	1.00

Table 6: Full correlation matrix

Allowing for background these statements may be expressed in the following equations. If ϵ_b, ϵ_c and ϵ_{uds} are the efficiencies for selecting different flavours in one hemisphere (where (uds)-quarks are not separated) and ϵ'_b, ϵ'_c and ϵ'_{uds} are the efficiencies for selecting events in which both hemispheres are tagged, then:

$$R_H = R_b \cdot \epsilon_b + R_c \cdot \epsilon_c + (1 - R_b - R_c) \cdot \epsilon_{uds} \quad (1)$$

$$\begin{aligned} R_E &= R_b \cdot \epsilon'_b + R_c \cdot \epsilon'_c + (1 - R_b - R_c) \cdot \epsilon'_{uds} \\ &= R_b \cdot \{\epsilon_b^2 + \rho_b \cdot (\epsilon_b - \epsilon_b^2)\} + R_c \cdot \epsilon_c^2 + (1 - R_b - R_c) \cdot \epsilon_{uds}^2 \end{aligned} \quad (2)$$

In these equations R_H is the fraction of tagged hemispheres, R_E the fraction of events in which both hemispheres are tagged and R_b, R_c are the fractions of $Z \to b\bar{b}$ and $Z \to c\bar{c}$ events respectively in the initial sample. It is assumed that hadronic decays of the Z consist of $b\bar{b}$, $c\bar{c}$ and light quark final states, so that the fraction of light quarks may be written as $R_{uds} \equiv (1 - R_b - R_c)$. The event efficiency for the b flavour, ϵ'_b, is expressed as: $\epsilon'_b = \epsilon_b^2 + \rho_b \cdot (\epsilon_b - \epsilon_b^2)$, which takes into account the correlation between hemispheres ρ_b. For c and uds flavours the tag efficiencies ϵ_c and ϵ_{uds} are small compared to ϵ_b so that the corresponding correlations do not influence R_b and ϵ_b and thus are not included in the above equations.

The fraction R_b and tagging efficiency ϵ_b can be extracted from equations (1-2) provided the values ϵ_c, ϵ_{uds}, ρ_b and R_c are known. The value of R_c can be taken from the standard model, while ϵ_c, ϵ_{uds}, ρ_b are extracted from the simulation. If the b-purity of

the tagged sample is high, the dependence on simulation is small and may be included in the systematic uncertainties.

The tagging technique used in this analysis is described in [24,25] and here we just mention the general features.

The tagging of the events containing b-hadrons is based on the fact that, because of the non-zero lifetime of hadrons with heavy flavour content, particle tracks from decays of such hadrons have large positive impact parameters [2] while tracks from the primary interaction have impact parameters which are smaller in absolute value and are equally likely to be positive or negative.

First a primary vertex was reconstructed. This was done using an iterative procedure starting with all tracks that were compatible with coming from the beam spot. The beamspot itself was used as an additional constraint. After that fit the vertex was recomputed dropping each track separately. The track with the largest χ^2 change was excluded if the change was larger than some threshold ($\Delta\chi^2 > 3$). This procedure was repeated until no change above threshold occurred. In about 1% of the events all tracks have been excluded this way. In these cases the beamspot position was used as primary vertex.

The tagging variable P_H [24,25] for selection of b-hadrons was defined for each hemisphere separately. It gives the probability for the particles in one hemisphere with their observed values of impact parameters to be all from the primary vertex. In this analysis we used tracks with positive impact parameters only in the definition of P_H. P_H varies from 0 to 1 and its main property is the flat distribution for hemispheres which do not contain the decays of long lived particles. Due to this property it can be named "hemisphere probability". P_H is constructed in such a way that the large impact parameters of the decay products of b-hadrons are transformed to a very low value of P_H. Thus events with b-hadrons can be tagged by selecting the hemispheres with P_H value less than some threshold. Different thresholds give different tagging efficiency and purity of the selected samples. The threshold position is arbitrary in this analysis and was chosen to minimize the total error of R_b . The independence of the measured value of R_b on the threshold position is an important cross-check for this technique. Figure 3 shows the distribution of $-\log_{10}(P_H)$ for the data and for different flavour contributions in the simulation.

The negative impact parameter distribution is determined mainly by the detector resolution and depends little on the dynamical properties of the event. It was used as the reference distribution of the particles from the primary interaction for the construction of the hemisphere probability. The calibration to the observed negative impact parameter distribution significantly simplified the comparison of data and simulation. The use of the impact parameter as the only quantity for the tagging of b-hadrons made the estimate of the background efficiencies more reliable.

The selection of tracks and events was as described in section 3. In the tagging algorithm only tracks with at least two VD hits have been used. In total 504197 hadronic events within the acceptance of vertex detector ($|\cos\theta_{thrust}| < 0.75$) were selected from the 1992 data sample which corresponds to an efficiency of about 71%. The bias of the b-flavour content in the selected sample is negligible ($(0.05 \pm 0.05)\%$) and was taken into account.

The tagging efficiency of events containing long lived particles depends significantly on the resolution of the tracking system. It was measured directly from the observed distribution of negative impact parameters requiring in addition that the event probability using tracks with positive impact parameter was larger than 0.1. In the simulation the resolution was corrected to fit the one obtained in the data.

[2] The sign of the impact parameter is defined to be positive if the crossing of the track and the axis of the fastest jet in the hemisphere lies in the direction of the track, else it is defined to be negative

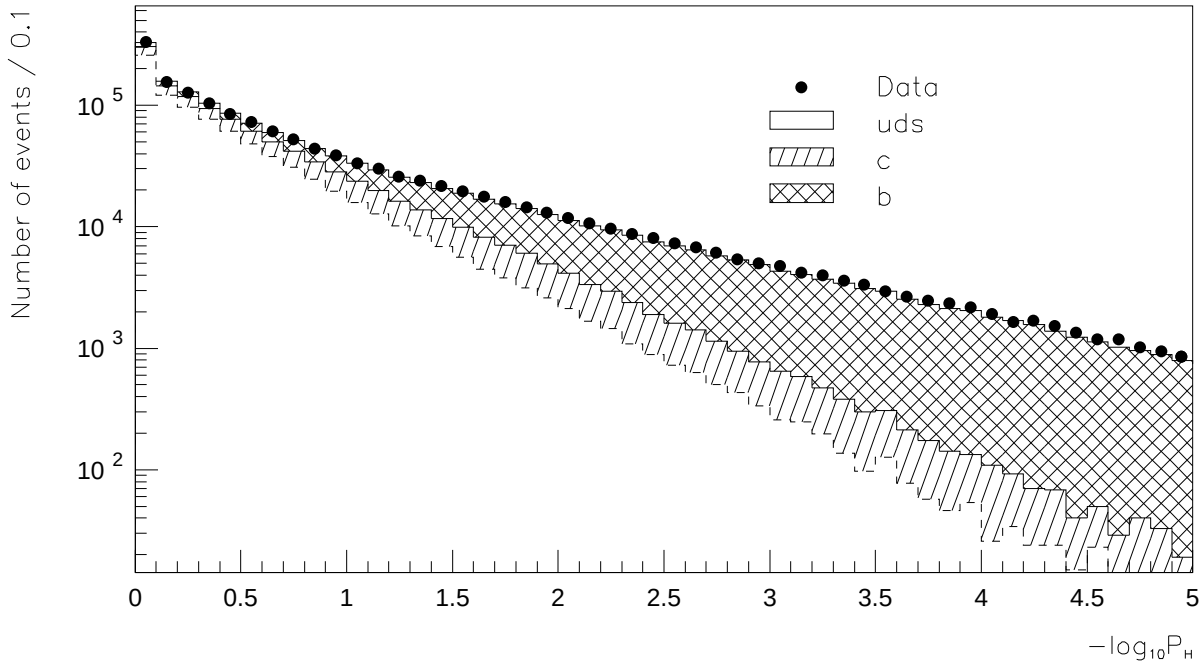

Figure 3: Distribution of $-\log_{10}(P_H)$ for the data and for different flavour contributions in the simulation corrected to have the same resolution as the data.

Source of systematics	$\Delta\epsilon_{uds} \times 10^4$
Detector resolution	± 2.2
K^0	± 0.8
Hyperons	± 0.3
Gluon splitting $g \to b\bar{b}$	± 0.3
Gluon splitting $g \to c\bar{c}$	± 0.1
Total	± 2.4

Table 7: Systematic errors of light quark efficiency ϵ_{uds}.

5.2 Estimates of Efficiencies and Correlations

For this measurement of R_b the tagging cut $-\log_{10}(P_H) > 2.7$, which gave a minimal total error, was used. The values of ϵ_c, ϵ_{uds}, ρ_b with this cut were extracted from the simulation and the possible sources of uncertainties were included as systematic errors.

The value of ϵ_{uds} was found to be:

$$\epsilon_{uds} = (0.323 \pm 0.006(stat) \pm 0.024(syst)) \times 10^{-2}. \quad (3)$$

The statistical error comes from the limited sample of simulated events used for estimation of ϵ_{uds}; the different sources of systematics are given in the Table 7.

The systematic error coming from the differences in resolution between data and simulation was estimated as the difference of the tagging efficiencies in data and in simulation when hemisphere probabilities were computed using tracks with negative impact parameters ("negative hemisphere probability"). Because tracks with negative impact parameters arise mainly from the resolution of the tracking system and do not contain

lifetime information, tagging with the negative hemisphere probability gives a good estimate of the component of light quark efficiency coming from statistical fluctuations of the impact parameter measurements.

The systematic error from the uncertainties in production of long lived particles in light quark events (K^0, Λ, hyperons) was obtained by varying the corresponding production rates in simulation by $\pm 10\%$. This variation corresponds to the observed differences between the production rate of these particles in data and simulation and agrees with the recommendations of [11]. The systematics from the gluon splitting $g \to b\bar{b}$ and $g \to c\bar{c}$ were obtained by varying the fraction of such events by $\pm 50\%$ [11]. In addition to these systematic sources, it was checked that the uncertainties from the interactions of particles in the material of the detector are negligible.

The efficiency to tag hemispheres with charm was found to be:

$$\epsilon_c = (1.70 \pm 0.03(stat) \pm 0.16(syst)) \times 10^{-2} \tag{4}$$

The simulation has been tuned to describe as well as possible the properties of charm production and decays as measured at LEP and at lower energies. For the evaluation of the systematic uncertainty the following parameters have been varied within their measurement error:

- the production ratios of the different charmed hadrons [11],
- the charged decay multiplicities of charmed hadrons [26],
- the inclusive branching ratios $D \to K^0 X$ [15],
- the c-hadron lifetimes [15],
- the mean energy of c-hadrons in fragmentation as measured by DELPHI [16].

For the central values and the errors we follow the prescription of [11]. The sources of systematic error are listed in table 8.

For the light quark efficiency mostly the accurate description of the resolution function in the probability calculation is important, assuring a flat distribution of the hemisphere probability. On the contrary, for charm the agreement between data and simulation is relevant, since tracks from charm decays have real impact parameters. An estimate of the uncertainty due to the knowledge of the detector resolution was obtained from the change in ϵ_c assuming the resolution curve obtained from the data in the calculation of the probabilities in the simulation. Since the error assignment to the impact parameters is the same in data and simulation the difference in the resolution curve reflects the difference in the true resolution.

The correlation between hemispheres in b events was evaluated to be

$$\rho_b = (-0.26 \pm 0.15(stat) \pm 0.09(syst)) \times 10^{-2}. \tag{5}$$

The correlation can be described mainly in term of four sources:

- Radiation of hard gluons: This source acts in two ways. Due to gluon radiation, energy is taken away from the b-hadrons, thus lowering the tagging efficiency. This leads to a positive correlation. In about 2% of the cases both b-hadrons are boosted into the same hemisphere, leading to a negative correlation.

Source of systematics	$\Delta\epsilon_c \times 10^4$
Detector resolution	± 10.2
Production rates of charm hadrons	± 9.9
Charged decay multiplicities	± 3.7
$D \to K^0 X$	± 4.9
Charmed hadrons lifetime	± 3.2
Fragmentation	± 2.7
Total	± 16.0

Table 8: Systematic errors of charm quark efficiency ϵ_c

- the polar angle of the thrust axis: Since both jets either are in a region of good or somewhat worse VD acceptance this leads to a positive correlation.

- the azimuthal angle of the jets: Due to dead or noisy modules in the vertex detector the efficiency was not flat in Φ. In the data sample presented here most modules have been highly efficient apart from few adjacent ones near $\Phi = 0$. Thus a bad module hit in one jet usually results in a good module hit in the other one. This leads to a negative correlation.

- the bias of the fitted production vertex due to the inclusion of tracks from b decays, leading to a negative correlation. The lifetime of the b-hadrons was found to be the best variable to describe this effect.

Figure 4 shows the total correlation as a function of the cut value, together with each of these four components and their sum.

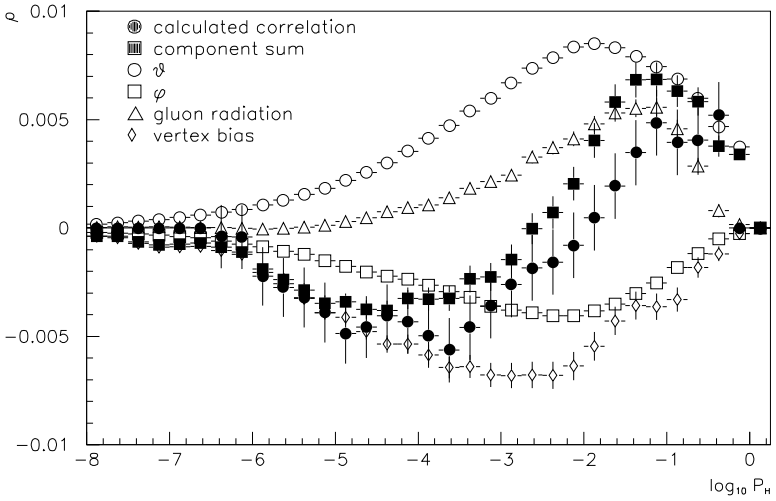

Figure 4: Total hemisphere correlation and individual contributions as a function of the cut value $\log_{10} P_H$.

Source of systematics	$\Delta\rho_b \times 10^4$
Resolution function	± 1.5
Polar angle acceptance	± 2.1
Azimuthal angle acceptance	± 6.5
Hard gluon emission	± 5.0
Lifetime of b-hadrons	± 3.3
total	± 9.2

Table 9: Systematic errors of correlation factor ρ_b.

To obtain the systematic error of the correlation estimate in the simulation from the first three sources, the fraction of tagged events was measured in data and in simulation using all events as a function of the relevant variable. From this the correlation due to the single variable considered was calculated. The result was scaled by the ratio of the correlations in $b\bar{b}$ and in all events obtained from the simulation. As the error estimate, the larger of either the difference between the data and simulation measurement or the error of this difference was taken. In the case of gluon radiation thrust was used as testing variable. This tested only the first aspect of the gluon radiation effect. However, it was checked with the simulation that the cancellation of the two effects does not depend on the assumptions made, so that the test done actually overestimates the error. For the vertex bias the b lifetime in simulation has been varied within the error of the current world average $\tau_B = 1.538 \pm 0.033 ps$ [27]. The different sources of the systematic errors are listed in the table 9.

5.3 Results

All the above values of efficiencies and correlation with their errors were substituted into equations (1) and (2). For R_c the standard model value was used with a relative error of 8% as suggested in [28] ($R_c = 0.171 \pm 0.014$).

The measured value of R_b is equal to:

$$R_b = 0.2224 \pm 0.0027(stat) \pm 0.0034(syst) \pm 0.0018(R_c). \qquad (6)$$

The b hemisphere tagging efficiency was found to be $\epsilon_b = 0.201 \pm 0.003$ compared to $\epsilon_b(MC) = 0.195$ obtained from the simulation. In equation (6) the systematic error coming from the value of R_c is separated from all other sources. A change in the value of R_c would change R_b by $\Delta R_b = -0.13 \times (R_c - 0.171)$. The breakdown of the error for the given cut on P_H is given in table 10.

As a cross-check of this measurement, the comparison of R_b values for different tagging cuts is given in Fig. 5. The measured value of R_b is stable over a wide range of variation of the efficiencies and correlation. The contribution of the different error sources, other than R_c, as a function of the cut value is shown in Fig. 6.

5.4 Combination with the 1991 Analysis

In order to combine the analysis presented here with a similar one made with the 1991 data [25], the following assumptions have been made:

- All statistical errors are assumed to be independent.

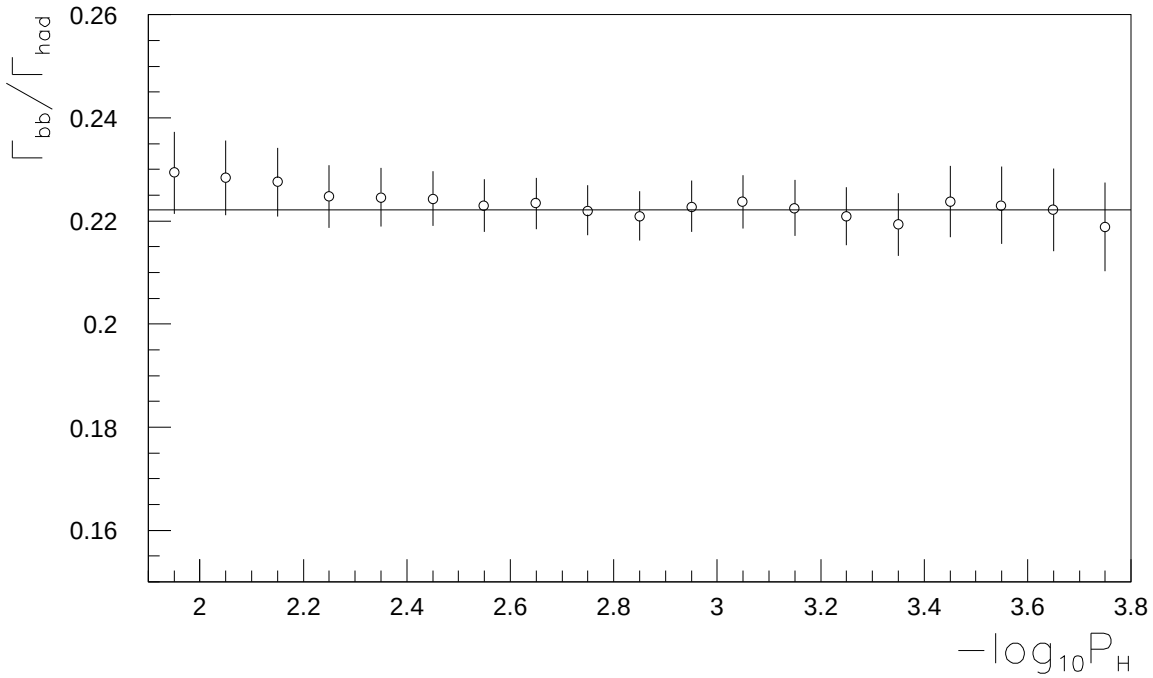

Figure 5: The value of $\Gamma_{b\bar{b}}\ /\Gamma_{had}$ with its total error as a function of the cut on $-\log_{10} P_H$. The straight line corresponds to the value measured at $-\log_{10} P_H > 2.7$.

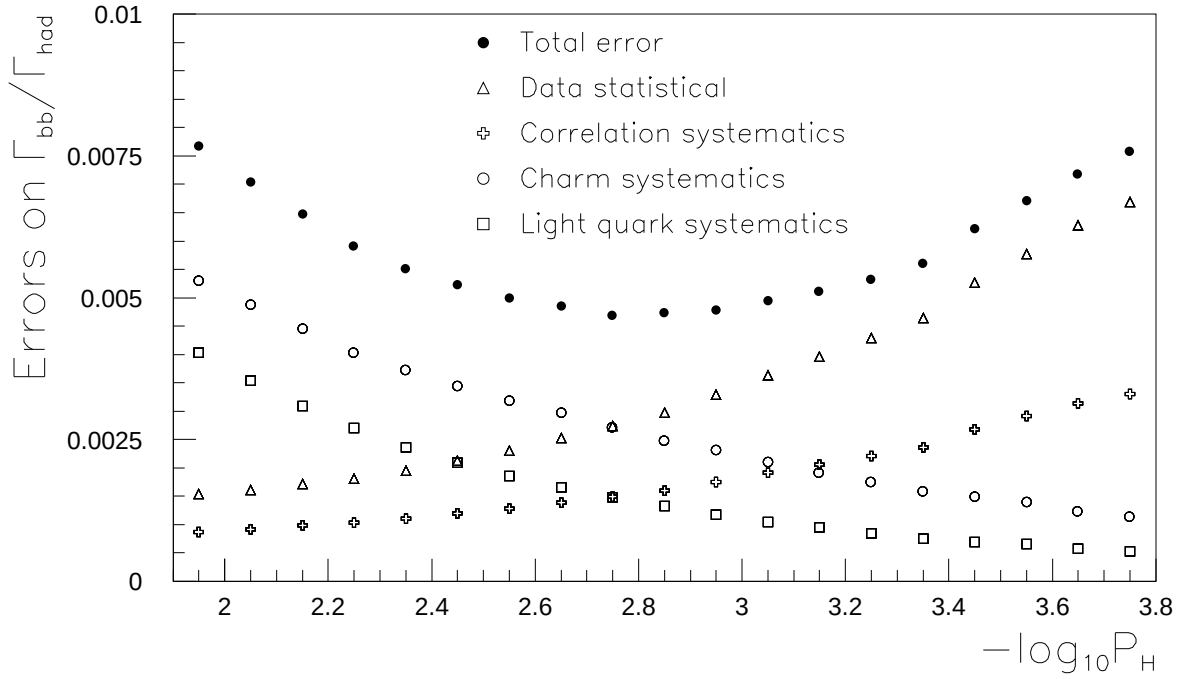

Figure 6: Contribution of the different error sources to the total error as a function of the cut on $-\log_{10} P_H$.

Error Source	$\Delta R_b \times 10^3$
Statistical error	± 2.74
Light quark efficiency	± 1.47
Charm efficiency	± 2.73
Correlation	± 1.49
$\Gamma_{c\bar{c}}$	± 1.80
Total	± 4.77

Table 10: Sources of errors for measurement of $R_b = \Gamma_{b\bar{b}}/\Gamma_{had}$.

- The errors in the hemisphere correlations due to hard gluon emission and b-hadron lifetimes are assumed to be fully correlated between the two years; the other errors contributing to hemisphere correlations are assumed to be independent.

- The errors due to resolution functions have been derived in a completely different way. The same is true for the tuning of the resolution function itself. They were thus also assumed to be independent.

- The error due to the modelling of the light quarks was assumed to be fully correlated.

- The error due to the modelling of the charm sector was derived in a slightly different way for the 1991 analysis. This error has been recalculated in the same way as for 1992 and was assumed to be fully correlated.

- The error due to the assumption on R_c was assumed to be fully correlated.

With these assumptions the result for the combined 1991 and 1992 data is:

$$R_b = 0.2217 \pm 0.0022(stat) \pm 0.0032(syst) \pm 0.0018(R_c) \qquad (7)$$

The breakdown of the error is given in table 15.

6 Mixed tag Analysis

The main statistical limitation of the presented analysis came from the relatively low number of double tagged events. A statistically practically uncorrelated measurement was performed by measuring the tag efficiency opposite to a high p_t lepton and then obtaining R_b from the single lifetime tag sample only. Also the systematic uncertainties turned out to be largely different in this case. This analysis is described in section 6.2.

Another analysis was performed by using a much more efficient lifetime tag with higher background. In this case the single and double lifetime tag sample together with the lepton tag one were used to measure the R_b, the b tagging efficiency and some background quantities from the data. This other analysis is described in section 6.3. Both the analyses were performed on the 1992 data sample only.

To extract with adequate precision the efficiency of the lifetime tags, both measurements required the accurate knowledge of the composition of the lepton sample, which is described in detail in the following section.

6.1 The Composition of the Lepton Sample

The results of the fit to the single and di-lepton distributions allowed a precise determination of the fraction P_b (P_c) of events from b (c) quarks in the lepton sample, by using the following formulae:

$$P_b = N_b/(N_b + N_c + N_{uds}) \quad (8)$$
$$P_c = N_c/(N_b + N_c + N_{uds}) \quad (9)$$

where N_q is the number of q flavored events ($q = b, c, uds$) in the kinematical domain considered. The fraction of leptons produced by light quarks (P_{uds}) was then obtained by imposing the condition: $P_{uds} + P_b + P_c = 1$. N_b was determined from the simulation after imposing the results of the lepton analysis (see section 4.3.3) adding the contributions from the leptons produced in primary and cascade b decays (see section 4.3.1) and from non-prompt sources in $b\overline{b}$ events. N_c includes leptons from direct c decays and from non-prompt sources in $c\overline{c}$ events, whereas only leptons from background sources contribute to N_{uds}. The errors on the results of the lepton analysis then contributed to the systematic error on the lepton sample composition. However, their overall effect is small due to the anticorrelation among some of the relevant parameters (particularly the one between R_b and bl, see table 4). The contribution to the systematic errors from the parameters which had not been determined in the lepton fit was evaluated by varying each of them as in section 4.3.3 (see tables 3 and 5).

The lepton purities were computed in the subset of hadronic events selected for the vertex analysis (see section 5.1) by means of equations (8) and (9) as a function of p_t. The most energetic candidate was used when more than one lepton was found in the event. The requirement $p_t > 1.5$ GeV/c was applied in order to minimize the overall error on R_b. The data sample consisted then of 14418 events. The purities of the sample were found to be:

$$P_b = (79.98 \pm 0.74)\%$$
$$P_c = (9.9 \pm 0.4)\%.$$

Table 11 shows the individual effect of all the considered error sources on P_b.

Source	ΔP_b
Monte Carlo statistics	± 0.27
Lepton Fit	± 0.34
Model $b \to l$	± 0.37
Model $c \to l$	± 0.29
$b \to \tau \to l$	± 0.03
$b \to \overline{c} \to l$	± 0.02
$b \to J/\Psi \to l$	± 0.03
$c \to l$	± 0.32
e misidentification	± 0.29
μ misidentification	± 0.21
e identification efficiency	± 0.06
μ identification efficiency	± 0.06

Table 11: Systematic errors (%) on the purity of the lepton sample, when the selection $p_t > 1.5$ GeV/c was applied to the lepton transverse momentum.

6.2 High Purity Analysis

This analysis used the same lifetime tagging technique as described in section 5.1. The simulation showed that the correlation between the b and $\bar{b}$ decay products was substantially reduced if the tags were performed on jets rather than on hemispheres. By grouping particles in jets rather than by hemispheres, the tracks from the radiated gluon are usually collected together in a unique jet so leaving the b and $\bar{b}$ jets well separated, and reducing the correlation among them. It was checked that for two jet events the jet and the hemisphere tags were equivalent.

Another effect was however observed. Jets were conventionally ordered on the basis of their energy. A correlation was observed between the energy of the b jet and the probability for it to be tagged. When a gluon was emitted, its jet was on average the least energetic one. However, when the third (fourth etc.) jet contained a lepton, it had greater chance to originate from a b quark than in unbiased events. This happened in $(5.46 \pm 0.08\%)$ of the real data and $(5.3 \pm 0.1\%)$ of the simulated ones. Such events were rejected.

For each jet in an event the tagging variable P_{jet} was then defined from all the tracks from charged particles belonging to the jet. It expresses the probability that all the tracks in the jet come from the primary vertex, as described in section 5. An event was considered as tagged if at least one jet satisfied the condition $P_{jet} < 4 \times 10^{-3}$.

In the sample of events where one jet was tagged by a high p_t lepton, the fraction having a different jet with a lifetime tag was:

$$R_{jet,l} \;=\; c_l^b \cdot \epsilon_b \cdot P_b \;+\; c_l^c \cdot \epsilon_c \cdot P_c \;+\; c_l^{uds} \cdot \epsilon_{uds} \cdot P_{uds} \tag{10}$$

This allowed to extract the efficiency ϵ_b of tagging a b jet, because the composition of the lepton sample was known (see section 6.1), while the efficiency of the c and uds tagging were estimated in the simulation as:

$$\begin{aligned} \epsilon_{uds} &= (1.05 \pm 0.01)\% \\ \epsilon_c &= (3.19 \pm 0.04)\% \end{aligned}$$

The coefficients c_l^q, arising from the residual correlations between the lepton and the lifetime tags, were computed in the simulation as well. Due to the small contaminations from c and light quarks, only the knowledge of c_l^b was relevant for the measurement.

Once the b tagging efficiency was determined, R_b was measured from the fraction of events having at least one b jet tagged, given by the following equation:

$$R_{jet} \;=\; R_b \cdot \epsilon_b + R_c \cdot \epsilon_c + (1 - R_b - R_c) \cdot \epsilon_{uds} \tag{11}$$

similar to (1). Table 12 reports, for a set of different probability cuts, the efficiency to tag a b jet expected in the unbiased $b\bar{b}$ events, compared to the one found when a lepton was present (simulation). Also shown is the efficiency for the data corrected for the correlation effects.

The good agreement between the measured and predicted efficiencies is a meaningful test of the precision of the procedure for the tuning of the impact parameters using the negative impact parameter distributions.

With the requirement $P_{jet} < 4 \times 10^{-3}$, 2889 events were selected, out of 14418 with the high p_t lepton, and a value:

$$R_b = 0.2223 \pm 0.0045$$

was derived, where the error is only statistical. The systematic errors will be discussed in section 6.4.

P_{jet} selection ($\times 10^{-3}$)	Simulation			data
	$\epsilon_{btag}(\%)$ (unbiased)	$\epsilon_{btag}(\%)$ (leptonic)	c_l^b	$\epsilon_{btag}(\%)$
0.50	12.45 ± 0.08	12.71 ± 0.10	1.021 ± 0.010	12.57 ± 0.36
1.90	20.05 ± 0.10	20.42 ± 0.12	1.018 ± 0.008	20.12 ± 0.45
4.00	25.92 ± 0.11	26.28 ± 0.13	1.014 ± 0.007	25.98 ± 0.50
6.00	29.78 ± 0.12	30.14 ± 0.13	1.012 ± 0.006	29.48 ± 0.52
8.50	33.18 ± 0.11	33.58 ± 0.14	1.012 ± 0.005	32.84 ± 0.54
10.00	35.29 ± 0.12	35.66 ± 0.14	1.010 ± 0.005	34.86 ± 0.55

Table 12: Jet b tag efficiency. The efficiency for unbiased $b\bar{b}$ events (second column) is compared to the one found in the lepton tagged sample using equation 10. The ratio c_l^b which is needed to correct the data and the corrected data are also shown

6.3 High Efficiency Analysis

In this analysis all the particles were grouped in hemispheres. In order to reduce the correlation between the two lifetime tags a separate primary vertex was computed in each hemisphere. The beam spot constraint was not imposed. The vertex was rejected if it was formed by less then three tracks from charged particles. The resolution in this case was symmetric in the two directions orthogonal to the beam directions: $\sigma_x = \sigma_y \simeq 100$ μm.

A hemisphere was considered as tagged if at least two charged particles were found in it with impact parameter δ satisfying the condition 0.1 mm $\leq |\delta| \leq$ 2.0 mm. The lower limit of this range reflects the sensitivity to the long b lifetime, and the upper limit removes a part of the background due to wrongly reconstructed primary vertices, particles from long lived strange particle decays and from photon conversions in the detector material.

All the available information was used in this case, inserting into equations (1) and (2), respectively the fraction of events in which at least one, or both, hemispheres had a lifetime tag, and into equation (10) the fraction of events with a mixed lepton-lifetime tag in opposite hemispheres. Due to the additional constraint, R_b, ϵ_b, and, in addition, the average efficiency to tag non-b quarks, $\epsilon_l = \frac{\epsilon_c R_c + \epsilon_{uds} R_{uds}}{R_c + R_{uds}}$, can be determined from the data. The ratio $\frac{\epsilon_c}{\epsilon_{uds}}$ had to be taken from simulation. However, due to the substantially higher background fraction in this analysis, the correlations for the light quarks ρ_c, ρ_{uds} could not be neglected. They were extracted from the simulation as:

$$\begin{aligned} \rho_b &= -0.0040 \pm 0.0045, \\ \rho_c &= 0.0037 \pm 0.0020, \\ \rho_{uds} &= 0.0021 \pm 0.0010, \end{aligned}$$

where the quoted errors come from the simulation statistics. The efficiency ratio was found to be $\frac{\epsilon_c}{\epsilon_{uds}} = 1.41 \pm 0.005$.

The coefficient c_l^b, expressing the effect of the correlation between the lifetime tag and the lepton tag in b events, was $c_l^b = 1.020 \pm 0.005$

Using these numbers the following value of R_b was found:

$$R_b = 0.213 \pm 0.007$$

The tagging efficiencies were $\epsilon_b = 0.599 \pm 0.005$ and $\epsilon_l = 0.264 \pm 0.002$.

6.4 Systematic Errors and Combination of the Results

The main sources of systematic errors which have to be considered for the mixed tag R_b measurement are:

a) uncertainties coming from the light quark efficiencies,

b) uncertainties coming from correlation effects,

c) uncertainties coming from the knowledge of the composition of the lepton sample.

For the high purity analysis errors from sources a) and b) have been evaluated exactly in the same way as in section 5. The effect of the unknowns on the light quark efficiencies turn out to be about a factor two smaller, since they enter only linearly in the equations determining R_b.

The error on the correlation between the lepton tag and the vertex tag is dominated by the limited statistics from simulation available. The two most relevant sources of correlation were the gluon radiation and the acceptance of the detectors involved. In fact, the gap between the barrel and forward muon chambers corresponds to a cos θ region were the VD sensitivity is reduced; in the same way the HPC polar acceptance overlaps with that of the micro-vertex detector (see section 2). As a consequence of this, when a jet happened to fall near the border of the sensitive region of the micro-vertex detector, the chance to miss the lepton in the opposite jets was higher. This induced a positive correlation between the two tags. No contribution was found due to the dead micro-vertex modules or to the reconstruction of the primary vertex (see section 5). The use of the jet tagging rather than the hemisphere tagging reduced the total amount of the correlation by a factor of about 2.

The same sources of uncertainty were also studied for the high efficiency analysis. Apart from them, the effect of the correlation between the vertex measurements in the two hemispheres must also be taken into account. The lifetime bias is removed because two different primary vertices are reconstructed. Some effects, due to variations of tagging efficiencies with global event variables (such as thrust direction, thrust value or time) were evaluated from the data, by fixing R_b to the measured value and measuring ϵ_b and ϵ_l by inverting the double tag system (equations (1-2) with the inclusion of all correlation factors), as a function of these variables. Instrumental effects due to acceptance correlation in the micro-vertex detector were also investigated. This was done by repeating the measurement in bins of $|\cos\theta_{thrust}|$ of size 0.1. The contribution to R_b was estimated by removing the last bin and performing the measurement again. In the same way, the Φ angular regions containing some micro-vertex dead modules (and the symmetrically opposite regions) were removed. The variation of R_b was taken in both cases as the systematic error. The effect of hard gluon radiation was evaluated from the simulation.

Details of the uncertainties in the purity of the lepton sample have been given above. These contributions were then added to the total error.

The value of R_c was varied as in section 5. The correlation between the high purity and high efficiency analysis was 54%. The average result was then:

$$R_b = 0.2216 \pm 0.0042(stat.) \pm 0.0039(syst.).$$

Table 13 gives the detailed contributions of all the sources of uncertainty considered above.

Source of error	δR_b		
	1st analysis	2nd analysis	combined
Statistical	± 0.0045	± 0.0070	± 0.0042
P_b	± 0.0022	± 0.0042	± 0.0023
P_c	± 0.0001	± 0.0002	± 0.0001
Resolution Function	± 0.0017	± 0.0010	± 0.0016
Vertex-lepton correlations	± 0.0018	± 0.0032	± 0.0019
R_c	± 0.0012	± 0.0012	± 0.0012
Charm efficiency	± 0.0013	± 0.0015	± 0.0013
uds-quarks efficiency	± 0.0007	± 0.0007	± 0.0007
Double vertex correlations	± 0.0000	± 0.0027	± 0.0002
Total	± 0.0059	± 0.0093	± 0.0057

Table 13: Contributions to the total error.

6.5 Consistency Checks

To test the understanding of the systematics, the analyses were repeated in different conditions. Each time, one of the relevant cuts was varied in order to check the stability of the results versus variations in the lepton sample composition, in the efficiency of the b tagging, and in the amount of background contamination.

- The cut on the lepton p_t was varied between 0 and 3 GeV/c for both analyses. Fig. 7 shows the dependence of the result on the p_t window considered for the method of section 6.2. The purity of b events varied from 20% to more than 80 % from the first to the last bin. Table 14 gives the evolution of the result of the method of section 6.3 as a function of the cut on p_t. A similar stability was also found when considering other variables, such as the lepton momentum, and the lepton polar and azimuthal angles, etc.

- The analysis of section 6.2 was repeated grouping the charged particles by hemispheres rather than by jets. The total correlation factor increased to $c_l^b = 1.029 \pm 0.005$. The variation on R_b was $+0.0018 \pm 0.0018$.

- The analysis of section 6.2 was repeated requiring probability less than 0.01 and then less than 0.0005. The efficiency of the tag, the fraction of background and the amount of correlation varied by more than a factor two. The value of R_b varied by $+0.0023 \pm 0.0022$ and -0.0037 ± 0.0047 respectively.

All the errors quoted are statistical only and take into account the statistical correlation between the samples compared. No apparent discrepancy was found.

7 Combination of the Results

The results from the lifetime analysis and mixed analysis (sections 5 and 6) have been combined taking into account the common systematic errors and the statistical correlations. The result is:

$$R_b = 0.2217 \pm 0.0020(stat) \pm 0.0029(syst) \pm 0.0016(R_c).$$

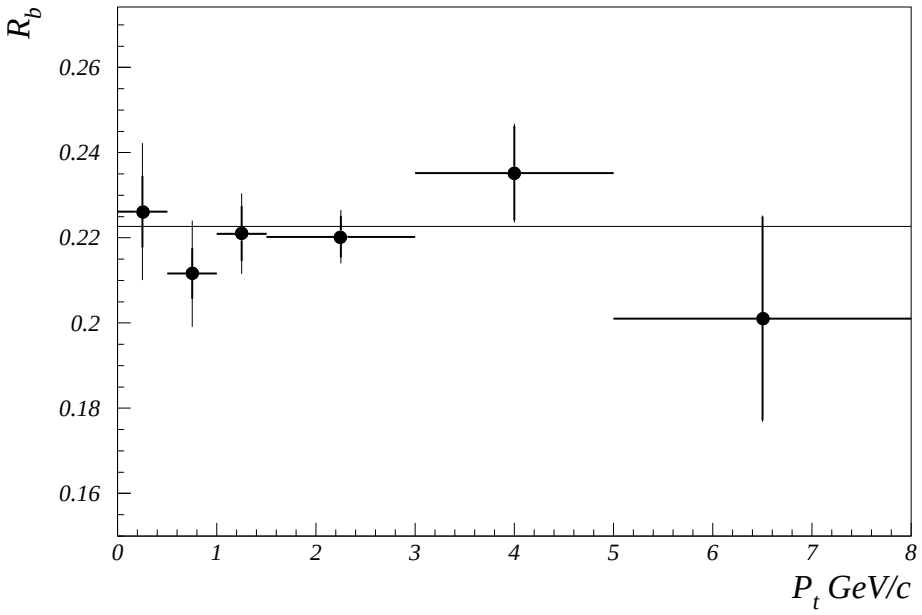

Figure 7: High purity analysis. R_b versus the transverse momentum of the lepton. The bins are uncorrelated. The fraction of events from b ranges from about 20 % in the first bin to more than 80% in the last ones. The statistical errors are marked. The line shows the result quoted in the text, obtained with the cut $p_t > 1.5$ GeV/c.

p_t^{cut} (GeV/c)	R_b	$(\Delta R_b)_{stat}$	$(\Delta R_b)_{syst}^{P_b,P_c}$
0	0.2151	$\pm$0.0048	$\pm$0.0115
0.5	0.2151	$\pm$0.0052	$\pm$0.0103
1.0	0.2156	$\pm$0.0061	$\pm$0.0074
1.5	0.2126	$\pm$0.0070	$\pm$0.0042
3.0	0.2265	$\pm$0.0160	$\pm$0.0040

Table 14: Evolution of R_b with the cut on the lepton transverse momentum, for the high efficiency analysis. The systematic error contains only the contributions due to the knowledge of P_b,P_c.

The breakdown of the error is given in table 15.

Finally also the lepton measurement (section 4) was included in the average, mainly to reduce the error on the branching ratio measurements. For this purpose a constrained fit was performed using the full correlation matrix of table 6 and imposing the precise measurement of R_b from the lifetime tags. For R_c the value predicted by the Standard Model was imposed. The result was:

$$\begin{aligned}
R_b &= 0.2210 \pm 0.0033 \pm 0.0003(model) \pm 0.0014(R_c) \\
BR(b \to l) &= (11.06 \pm 0.39 \pm 0.19(model) \pm 0.12(R_c))\%, \\
BR(b \to c \to l) &= (7.70 \pm 0.97 \pm 0.33(model) \pm 0.32(R_c))\%, \\
\langle x_E \rangle &= 0.7030 \pm 0.0076 \pm 0.0037(model) \pm 0.(R_c), \\
\chi_b &= 0.150 \pm 0.024 \pm 0.004(model) \pm 0.001(R_c).
\end{aligned}$$

Error Source	Range	Uncertainty dvt	mt	comb.
Internal experimental effects:				
Hemisphere correlations		± 0.0014	± 0.0001	± 0.0010
Lepton-vertex correlations		0	± 0.0019	± 0.0005
Resolution function		± 0.0016	± 0.0016	± 0.0016
Lepton sample purity		0	± 0.0017	± 0.0005
acceptance bias		± 0.0003	0	± 0.0002
$\langle x_E(c) \rangle$	0.49 ± 0.02	∓ 0.0005	∓ 0.0004	∓ 0.0005
$\mathrm{Br}(c \to \ell)$	$(9.8 \pm 0.5)\%$	0	± 0.0009	± 0.0003
Semilept. model $b \to \ell$ [11]	$(^{+\mathrm{ACCMM}}_{-\mathrm{ISGW}^{**}})$	0	± 0.0010	± 0.0003
Semilept. model $c \to \ell$ [11]	ACCMM1 $(^{+\mathrm{ACCMM2}}_{-\mathrm{ACCMM3}})$	0	∓ 0.0008	∓ 0.0002
D^0 fraction in $c\bar{c}$ events	0.557 ± 0.053	∓ 0.0001	∓ 0.0001	∓ 0.0001
D^+ fraction in $c\bar{c}$ events	0.248 ± 0.037	∓ 0.0013	∓ 0.0008	∓ 0.0012
$(D^0 + D^+)$ fraction in $c\bar{c}$ events	0.80 ± 0.07	∓ 0.0008	∓ 0.0005	∓ 0.0007
D_s fraction in $c\bar{c}$ events	0.15 ± 0.03	∓ 0.0006	∓ 0.0004	∓ 0.0005
D^0 lifetime	0.420 ± 0.008 ps	∓ 0.0003	∓ 0.0002	∓ 0.0003
D^+ lifetime	1.066 ± 0.023 ps	∓ 0.0004	∓ 0.0002	∓ 0.0004
D_s lifetime	$0.450^{+0.030}_{-0.026}$ ps	∓ 0.0003	∓ 0.0002	∓ 0.0003
Λ_c lifetime	$0.191^{+0.015}_{-0.012}$ ps	0	0	0
D decay multiplicity	2.53 ± 0.06	∓ 0.0006	∓ 0.0004	∓ 0.0005
$BR(D \to K^0 X)$	0.46 ± 0.06	± 0.0008	± 0.0005	± 0.0007
$g \to b\bar{b}$ per multihadron	$(0.18 \pm 0.09)\%$	∓ 0.0002	∓ 0.0002	∓ 0.0002
$g \to c\bar{c}$ per multihadron	$(1.3 \pm 0.7)\%$	∓ 0.0001	∓ 0.0001	∓ 0.0001
Rate of long-lived light hadrons	Tuned JETSET$\pm 10\%$	∓ 0.0009	∓ 0.0007	∓ 0.0008

Table 15: Summary of systematic errors on R_b obtained from the double vertex tag (dvt, section 5) the mixed tag (mt, section 6) and the combination of the two analyses. Detailed explanations how the different error sources are obtained can be found in [11].

The first error contains the total experimental error and most of the modelling uncertainties, the second is half the difference between the result using the ACCMM and the IGSW** model for the semileptonic b decays and the third is due to the variation of R_c as in section 5.3. In a dedicated study [23] DELPHI measured $\chi_b = 0.121 \pm 0.016$ within the ACCMM model. This number is in agreement with number presented here (0.146 ± 0.024 in the same model) but more precise. The analysis presented in [23] could use less tight requirements on the availability of the lepton identification system than the one presented here. Also the simulated event sample was used in a way more optimized for the mixing analysis. In addition in [23] all input parameters have been used from world averages instead of determining some of them in the same fit.

8 Conclusions

Four different measurements of the partial decay width R_b of the Z into b-hadrons have been performed. Events were selected either by leptons carrying high transverse momentum or with tracks having a large impact parameter. From the lepton only analysis

also R_c, the semileptonic branching ratio $BR(b \to l)$ and other properties of b-events were measured. From the different analyses the following results were obtained:

Lepton analysis:

$$\begin{aligned}
R_b &= 0.2145 \pm 0.0089(stat) \pm 0.0063(exp.sys.) \pm 0.0023(model), \\
BR(b \to l) &= (11.41 \pm 0.45(stat) \pm 0.50(exp.sys.) \pm 0.34(model))\%, \\
BR(b \to c \to l) &= (7.36 \pm 0.49(stat) \pm 0.95(exp.sys.) \pm 0.57(model))\%, \\
R_c &= 0.1623 \pm 0.0085(stat) \pm 0.0168(exp.sys.) \pm 0.0124(model), \\
\langle x_E \rangle &= 0.7020 \pm 0.0044(stat) \pm 0.0021(exp.sys.) \pm 0.0071(model), \\
\chi_b &= 0.154 \pm 0.020(stat) \pm 0.010(exp.sys.) \pm 0.011(model).
\end{aligned}$$

Double lifetime tag:

$$R_b = 0.2217 \pm 0.0022(stat) \pm 0.0032(syst) \pm 0.0018(R_c).$$

High purity mixed tag:

$$R_b = 0.2223 \pm 0.0045 \pm 0.0034(syst) \pm 0.0012(R_c).$$

High efficiency mixed tag:

$$R_b = 0.2130 \pm 0.0070 \pm 0.0062(syst) \pm 0.0012(R_c).$$

The R_c error always corresponds to a R_c variation of 8% around its Standard Model value.

Combining all numbers the following results are obtained:

$$\begin{aligned}
R_b &= 0.2210 \pm 0.0033 \pm 0.0003(model) \pm 0.0014(R_c), \\
BR(b \to l) &= (11.06 \pm 0.39 \pm 0.19(model) \pm 0.12(R_c))\%, \\
BR(b \to c \to l) &= (7.70 \pm 0.97 \pm 0.33(model) \pm 0.32(R_c))\%, \\
\langle x_E \rangle &= 0.7030 \pm 0.0076 \pm 0.0037(model) \pm 0.(R_c),
\end{aligned}$$

The first error is the total error apart from the model uncertainties on the shapes of the lepton spectra from b decays and the uncertainty on the partial decay width of the Z to charm hadrons which are given separately. All results are in agreement with those of other measurements at LEP [21,29–32]. Assuming a mass of the top quark of $m_t = 174 \pm 17$ GeV as suggested by a measurement of the CDF collaboration [33] the Standard Model predicts $R_b = 0.2157 \mp 0.0006$ [34] whereas R_c does not depend significantly on other parameters. This number agrees to 1.5 standard deviations with our measurement assuming $R_c = 0.171$.

Acknowledgements

We are greatly indebted to our technical collaborators and to the funding agencies for their support in building and operating the DELPHI detector, and to the members of the CERN-SL Division for the excellent performance of the LEP collider.

References

[1] See, for example,
J.H. Kühn, P.M. Zerwas, in: *Z Physics at LEP 1*, eds. G. Altarelli, R. Kleiss and C. Verzegnassi, Vol. 1 (CERN 89-08, 1989) pp. 271-275.

[2] DELPHI Collaboration, P. Aarnio et al., Nucl. Inst. Meth. **A303** (1991) 233.

[3] N. Bingefors et al., Nucl. Inst. Meth. **A328** (1993) 447.

[4] T. Sjöstrand et al., in *"Z physics at LEP 1"*, CERN 89-08, CERN, Geneva, 1989. Comp. Phys. Comm. **39** (1986) 347.

[5] DELSIM Reference Manual, DELPHI 87-98 PROG 100, Geneva, 1989.

[6] JADE Collaboration, W.Bartel et al., Z. Phys. **C33** (1983) 23; S.Bethke et al., Phys. Lett. **B213** (1988) 235.

[7] G. Pistolato, F. Simonetto, *A Study of The Background to The Semileptonic Decays of Heavy Favours* DELPHI 94-7 Phys 352.

[8] N. Isgur et al., Phys. Rev. **D39** (1989) 799.

[9] CLEO Collaboration, S. Henderson et al., Phys. Rev. **D45** (1992) 2212.

[10] G. Altarelli et al., Nucl. Phys. **B208** (1982) 365.

[11] The LEP Electroweak Working Group, ALEPH Note 94-30, DELPHI 94-23 Phys 357 , L3 Note 1577, OPAL Technical Note TN213 , 28 February, 1994;
The LEP Electroweak Working Group, ALEPH note 94-90, DELPHI 94-23 Phys 357/add , L3 Note 1613, OPAL Technical Note TN237 , 10 June, 1994 .

[12] CLEO Collaboration, D. Bortoletto, et al., Phys. Rev. **D45** (1992) 21.

[13] ALEPH Collaboration, D. Buskulic et al., Phys. Lett. **B298** (1993) 479.

[14] ARGUS Collaboration, H. Albrecht et al., Phys. Lett. **B278** (1992) 202.

[15] Particle Data Group - Review of Particle Properties - Phys. Rev. **D45** (1992) 1.

[16] DELPHI Collaboration, P.Abreu et al., Z. Phys. **C59** (1993) 533.

[17] C.Peterson et al., Phys.Rev. **D27** (1983) 105.

[18] P. Collins and T. Spiller, J.Phys. **G11** (1985) 1289.

[19] V.G. Kartvelishvili, A.K. Likhoded , V.A. Petrov, Phys. Lett. **B78** (1978) 615.

[20] M. Bauer et al., Z. Phys. **C34** (1987) 103.

[21] OPAL Collaboration, R. Akers et al., Z. Phys. **C60** (1993) 199.

[22] R. Barlow et al., Comp. Phys. Comm. **77** (1993) 219.

[23] DELPHI Collaboration, P.Abreu et al., Phys. Lett. **B332** (1994) 488.

[24] G. Borisov, *Lifetime Tag of events $Z \to b\bar{b}$ with the DELPHI detector* IHEP 94-98, 1994.

[25] DELPHI Collaboration, P.Abreu et al., *Measurement of the $\Gamma_{b\bar{b}}/\Gamma_{had}$ Branching Ratio of the Z by Double Hemisphere Tagging* , CERN–PPE/94–131 , to be published in Z. Phys. C.

[26] D. Coffman et al., (MARK III Collaboration), Phys.Lett. **B263** (1991) 135.

[27] S. Squarcia, *Heavy Flavour Physics at LEP*, CERN-PPE/94-69.

[28] The LEP Collaborations, *Updated Parameters of the Z Resonance from Combined Preliminary Data of the LEP Experiments*, CERN-PPE/93-157.

[29] ALEPH Collaboration, D. Buskulic et al., Phys. Lett. **B313** (1993) 535.

[30] OPAL Collaboration, P.D. Acton et al., Z. Phys. **C65** (1995) 17.

[31] ALEPH Collaboration, D. Buskulic et al., Z. Phys. **C62** (1994) 179.

[32] L3 Collaboration, O. Adriani et al., Phys. Lett. **B307** (1993) 237.

[33] CDF Collaboration, F. Abe et al., Phys. Rev. Lett. **73** (1994) 225.

[34] D. Bardine et al., *ZFITTER: An Analytical Program for Fermion Pair Production in e^+e^- Annihilation*, CERN-TH 6443/92 (May 1992).